# Microbial network stability, not diversity, drives colonization resistance against Borrelia afzelii in Ixodes ricinus ticks

Lianet Abuin-Denis, Lourdes Mateos-Hernández, Apolline Maitre, Alejandra Wu-Chuang, Myriam Kratou, Salma Kaoutar Abdelali, Ana Laura Cano-Argüelles, Štefánia Skičková, Dasiel Obregon, Alina Rodríguez-Mallon, et al.

Ticks and Tick-borne Diseases 17 (2026) 102613

Contents lists available at ScienceDirect

Ticks and Tick-borne Diseases

journal homepage: www.elsevier.com/locate/ttbdis

Original article

# Microbial network stability, not diversity, drives colonization resistance against *Borrelia afzelii* in *Ixodes ricinus* ticks

Lianet Abuin-Denis [a,b], Lourdes Mateos-Hernández [a], Apolline Maitre [a], Alejandra Wu-Chuang [a], Myriam Kratou [c], Salma Kaoutar Abdelali [d], Ana Laura Cano-Argüelles [e], Štefánia Skičková [f], Dasiel Obregon [g], Alina Rodríguez-Mallon [b], Alejandro Cabezas-Cruz [b,*]

[a] ANSES, INRAE, Ecole Nationale Vétérinaire d'Alfort, UMR BIPAR, Laboratoire de Santé Animale, Maisons-Alfort, F-94700, France
[b] Animal Biotechnology Department, Center for Genetic Engineering and Biotechnology, Avenue 31 between 158 and 190, P.O. Box 6162, Havana 10600, Cuba
[c] Laboratory of Microbiology, National School of Veterinary Medicine of Sidi Thabet, University of Manouba, Manouba, 2010, Tunisia
[d] Laboratory of Research on the Improvement and Development of Animal and Plant Production, University of Ferhat Abbas, Setif, Algeria
[e] Parasitology Laboratory, Institute of Natural Resources and Agrobiology of Salamanca (IRNASA, CSIC), Cordel de Merinas, 40-52, 37008 Salamanca, Spain
[f] Pavol Jozef Šafárik University in Košice, Faculty of Science, Košice, Slovakia
[g] School of Environmental Sciences, University of Guelph, Guelph, ON, Canada

ARTICLE INFO

*Keywords:*
*Borrelia afzelii*
*Ixodes ricinus*
Colonization resistance
Microbial network stability
Tick microbiome

ABSTRACT

Most tick-borne pathogens (TBPs) are acquired secondarily, when ticks feed on infected hosts, meaning the pathogen must establish itself within an already assembled microbiota. These scenarios are subject to "priority effects," where the order of microbial arrival influences the success of later colonizers. Microbial interactions within arthropod vectors can therefore shape infection outcomes, producing either infection-refractory states, where resident microbes and their interactions reduce the likelihood of pathogen establishment, or infection-permissive states, where such barriers are absent or weakened and the pathogen establishes infection successfully. Hamilton et al. (2021) assessed larval microbiota before pathogen exposure and sequenced the microbiota of fed nymphs, both exposed or not to *Borrelia afzelii*, enabling priority-effect hypotheses to be tested. Despite uniform exposure to the highly infectious *B. afzelii* strain NE4049, only a subset of ticks became *Borrelia*-positive, suggesting refractory and permissive microbiota states. We reanalyzed the original dataset to test whether differences in microbiome community assembly and co-occurrence network features, beyond diversity metrics, were associated with these states. Refractory nymph networks exhibited higher connectivity and structural resilience, with *Staphylococcus* emerging as a central taxon already present in unfed larvae. In contrast, permissive networks showed reduced robustness and a marginal role for *Staphylococcus*. Notably, dysbiosis altered microbial assembly but did not prevent network reconfiguration in refractory ticks. Our findings suggest that colonization resistance is better explained by microbial network integrity than by diversity alone. Methodologically, they show that integrating community assembly theory and network analyses can reveal key features of the tick microbiota associated with vector competence.

## 1. Introduction

Ticks are obligate hematophagous arthropods that serve as vectors for a wide range of tick-borne pathogens, including bacteria, viruses, and protozoa, impacting both human and animal health (de la Fuente et al., 2017). Tick-borne diseases, such as Lyme borreliosis, have been increasing in prevalence, highlighting the need to better understand the ecological and microbial factors influencing pathogen transmission. Lyme borreliosis is caused by tick-borne spirochetes that belong to the *Borrelia burgdorferi sensu lato* genospecies complex and members include *Borrelia burgdorferi* sensu stricto (s.s.) and *Borrelia afzelii*. In Europe, *B. afzelii* is transmitted by *Ixodes ricinus*, whereas in North America, *Borrelia burgdorferi* s.s. is transmitted by *Ixodes scapularis* (Radolf et al., 2012). During the tick life cycle, *Borrelia burgdorferi sensu lato* (s.l.)

* Corresponding author.
*E-mail address:* alejandro.cabezas@vet-alfort.fr (A. Cabezas-Cruz).

https://doi.org/10.1016/j.ttbdis.2026.102613
Received 23 March 2025; Received in revised form 28 January 2026; Accepted 1 February 2026
Available online 14 February 2026

pathogens are typically acquired at the larval stage during a blood meal on an infected vertebrate host. After acquisition, *B. burgdorferi* s.l. spirochetes colonize the tick midgut and persist through the molt into the nymphal stage, at which point they can be transmitted to a new host during the next blood meal (Piesman and Gern, 2004).

Once inside the tick, *Borrelia* must navigate complex ecological interactions within the tick gut, where it encounters a diverse microbiota. Early work provided experimental evidence for a microbiota–immunity–colonization axis: broad disruption of the *Ixodes scapularis* larval gut microbiota reduced *Borrelia burgdorferi* colonization and was associated with decreased JAK/STAT signaling and compromised peritrophic matrix integrity, a barrier feature that the spirochete exploits to persist in the midgut (Narasimhan et al., 2014). Complementing this, subsequent work showed that the tick *I. scapularis* actively maintains gut microbiota homeostasis through immune effector mechanisms—e.g., the secreted gut protein PIXR limits bacterial biofilm formation and shapes gut microbiome/metabolome/immune responses in ways that favor efficient *B. burgdorferi* colonization, illustrating how immune regulation of the microbiota can create permissive conditions for infection (Narasimhan et al., 2017).

More recent studies refine this picture by moving from global dysbiosis to taxon-informed perturbation and reveal the reciprocal direction as well (infection→microbiota): *Borrelia* infection can modulate microbiota composition and—critically—community assembly structure, and departures from this pathogen-associated microbiota state induced by anti-microbiota antibodies or introduction of novel commensals reduce *B. afzelii* loads; network analyses identify interaction-level properties that better define infection-refractory microbiota states than diversity metrics alone (Wu-Chuang et al., 2023). Mechanistically, anti-microbiota vaccination targeting keystone bacterial groups provides a tractable route to pinpoint specific microbial components and downstream host responses: such immunization reshapes co-occurrence network structure and resistance to taxa removal in a taxon-specific manner (Mateos-Hernández et al., 2021)and can further drive metabolite–immunity coupling (e.g., lysine elevation and defensin induction with anti-*Borrelia* activity) that reduces colonization without requiring large changes in conventional diversity measures (Mateos-Hernandez et al., 2025).

At the same time, work using multiple non–taxon-specific strategies to perturb environmentally acquired microbiota (including germ-free rearing and other global perturbations) indicates that such broad shifts do not substantially influence spirochete migration from the midgut or transmission to the vertebrate host, consistent with the idea that later infection stages may be less exposed to luminal microbiota than colonization itself (Narasimhan et al., 2022).

These findings suggest that the microbiota–immune axis shapes *Borrelia* colonization in a manner that is often interaction- and function-dependent, motivating a shift from diversity/composition summaries toward community assembly and network-level properties as the relevant explanatory layer.

Community assembly describes the processes through which microbiomes are formed, maintained, and reconfigured, integrating host immune regulation, environmental filtering, and biotic interactions with stochastic effects such as dispersal and historical contingency (Obregon et al., 2025). In ticks, assembly processes including priority effects (Maitre et al., 2023), immune-mediated filtering (Mateos-Hernandez et al., 2025), and interaction rewiring operate across developmental stages and can generate alternative microbiota states that differ in their compatibility with pathogen colonization (Abuin-Denis et al., 2024a). Tick microbiome assembly is strongly shaped by early-life conditions, blood-meal–induced remodeling, and host immune regulation, all of which influence microbial interaction networks and the stability of community organization (Obregon et al., 2025). Broad or non-targeted perturbations—such as early-life dysbiosis (Narasimhan et al., 2014) or blood feeding (Hamilton et al., 2021) on infected hosts—can disrupt interaction structure and reduce network robustness, generating microbiota states more permissive to pathogen establishment. In contrast, taxon-informed manipulation of specific microbial components, including anti-microbiota interventions, can reorganize interaction networks into alternative, infection-refractory assembly states, in which resistance emerges from altered interaction structure, keystone taxa dynamics, and network robustness rather than from changes in overall diversity (Wu-Chuang et al., 2023). Consistent with this, tick microbiotas characterized by cohesive interaction networks, modular organization, and high resistance to perturbation are more likely to remain refractory to invasion despite equivalent pathogen exposure (Abuin-Denis et al., 2024b). Together, these considerations motivate a shift toward community assembly– and network-based approaches that explicitly capture interaction structure, robustness, and vulnerability to perturbation as key determinants of tick vector competence.

Despite these advances, empirical tests of community assembly–based hypotheses in tick–*Borrelia* systems remain limited, largely because most experimental designs focus on group-level microbiome shifts rather than outcome-resolved comparisons under controlled exposure. In particular, few studies explicitly leverage the natural variation in infection outcomes that occurs when ticks experience identical exposure to *Borrelia* yet differ in whether colonization is successfully established. Such contrasts offer a powerful opportunity to identify microbiota states that are compatible with, or refractory to, pathogen establishment, independent of exposure, host, or pathogen strain.

A uniquely well-suited dataset to address this gap was generated by Hamilton et al. (2021), who experimentally manipulated the microbiota of immature *I. ricinus* ticks and exposed larvae to *B. afzelii*–infected hosts, demonstrating that larval feeding on infected mice induces persistent, host-mediated changes in the tick microbiome that carry through the molt. Notably, although all larvae feeding on infected mice were exposed to the same pathogen source, only a subset of the resulting nymphs became infected, while others remained uninfected. While the original study established infection-associated microbiome shifts at the group level, it did not examine which microbiota features distinguished ticks in which *Borrelia* successfully established from those in which exposure did not result in infection. Taken together, this experimental design enables a complementary and previously unexplored question: among ticks that experienced identical exposure to *Borrelia*, which microbiota states are associated with successful versus unsuccessful colonization? By explicitly contrasting ticks that fed on the same infected hosts yet diverged in infection outcome, this framework allows microbiota features associated with permissive and refractory outcomes to be examined independently of exposure, host, or pathogen strain.

Here, we reanalyze this dataset through a community assembly framework to test the hypothesis that differences in microbiota interaction structure and assembly underlie divergent colonization outcomes following identical exposure. Specifically, we hypothesize that ticks exhibiting refractory outcomes harbor microbiotas characterized by cohesive interaction networks and greater structural robustness, whereas permissive outcomes are associated with disrupted community assembly and reduced network stability, rendering these microbiotas more compatible with *Borrelia* establishment. By leveraging this existing dataset at higher ecological resolution, our study aims to extract additional biological insight from an experimentally robust design, rather than to reassess its original conclusions.

## 2. Materials and methods

### 2.1. Original data sets

The published datasets from the study by Hamilton et al. (2021) were used in the present analysis. The purpose of the study by Hamilton et al. (2021) was to determine whether the larval microbiome influenced the vector competence of immature *I. ricinus* ticks for *B. afzelii*. Each of 10 female *I. ricinus* ticks that had fed on roe deer were allowed to lay their

eggs in the lab. For each female tick, the eggs were split in two batches, one batch of eggs was surface sterilized with bleach to remove the bacteria on the egg surface and the other batch was rinsed with water. The manipulation of the larval microbiome was successful as the control larvae that hatched from untreated eggs had 27.5x more bacteria (measured by qPCR of the *16S rRNA* gene) compared to the dysbiosed larvae that hatched from surface-sterilized eggs. These two types of larvae were fed either on mice infected with *B. afzelii* strain NE4049 ($n$ = 20) or uninfected control mice ($n$ = 20). The engorged larvae were allowed to moult into unfed (flat) nymphs, which were frozen at 4 weeks after the larva-to-nymph moult (Fig. 1). DNA was extracted from the 4-week-old nymphs ($n$ = 370) and qPCR was used to determine the presence and spirochete load of *B. afzelii*. For the nymphs that had fed as larvae on the infected or the uninfected mice, the infection prevalence was 71.0 % (130/183) and 2.85 % (3/106), respectively (Hamilton et al., 2021).

Prior to DNA extraction, the nymphs were either washed with ethanol to remove the surface bacteria or left unwashed (Fig. 1). The tick microbiome was characterized using metagenomic sequencing of the bacterial *16S rRNA* gene. The first PCR amplified a 464-bp fragment of the V3-V4 region of the 16S rRNA gene using specific primers and Illumina adapters. The second PCR added sample barcodes using similar reagents and conditions. After purification, 384 amplicons were pooled in equimolar concentrations and sequenced on an Illumina MiSeq v2 (Hamilton et al., 2021).

For our analysis, we restricted the dataset to ethanol-washed ticks to standardize decontamination procedures and reduce the contribution of surface-derived taxa. Our datasets were categorized into different groups: control larvae ($n$ = 18), dysbiosed larvae ($n$ = 19), control-normal nymphs ($n$ = 44, nymphs from control larvae fed on control mice), permissive-normal nymphs ($n$ = 28, nymphs molting from control larvae fed on infected mice and positive for *B. afzelii* infection), refractory-normal nymphs ($n$ = 13, nymphs molting from control larvae fed on infected mice but negative for *B. afzelii* infection), control-dysbiosed nymphs ($n$ = 32, nymphs molting from dysbiosed larvae fed on control mice), permissive-dysbiosed nymphs ($n$ = 36, nymphs molting from dysbiosed larvae fed on infected mice and positive for *B. afzelii* infection) and refractory-dysbiosed nymphs ($n$ = 10, nymphs molting from dysbiosed larvae fed on infected mice and negative for *B. afzelii* infection) (Fig. 1). This classification allowed us to identify differences in microbiota diversity, composition, and community structure between ticks exposed to *B. afzelii* and those actively carrying it.

### 2.2. Bioinformatic processing of raw sequences

The sequences were downloaded from the NCBI BioProject

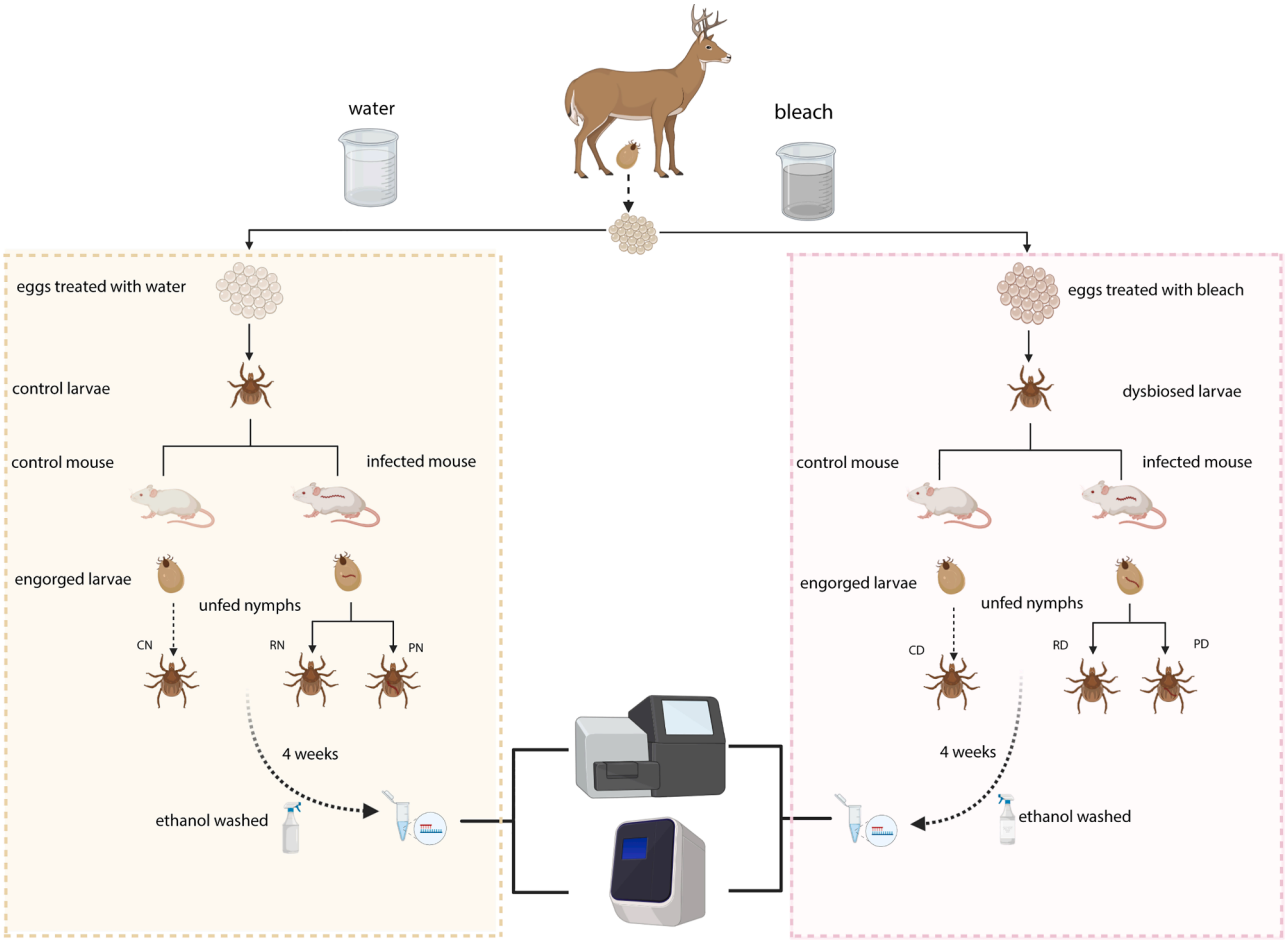


**Fig. 1.** Experimental design and grouping of Ixodes ricinus ticks used for microbiota analyses.
Engorged adult female I. ricinus ticks were collected from roe deer and allowed to lay eggs in a controlled phytotron. One batch of eggs was treated with water, generating control larvae, and the other batch was surface-sterilized with bleach, generating dysbiosed larvae. Each larval group was divided and fed either on Borrelia afzelii-infected mice or on uninfected control mice. Engorged larvae were collected and allowed to molt into unfed nymphs under controlled conditions. After four weeks, unfed nymphs were rinsed with ethanol before DNA extraction. DNA from larvae and nymphs was used for Borrelia detection and 16S rRNA gene amplicon sequencing to characterize microbiota composition and network structure. We generated eight experimental groups: larvae-control (CL), larvae dysbiosed (LD), control-normal (CN), permissive-normal (PN), and refractory-normal (RN) nymphs derived from water-treated eggs; and control-dysbiosed (CD), permissive-dysbiosed (PD), and refractory-dysbiosed (RD) nymphs derived from bleach-treated eggs. Fig. created with BioRender.com.

PRJNA732915, extracted, and de-interlaced in two fastq datasets containing the forward and reverse mate reads. Using DADA2 software (Callahan et al., 2016) implemented in Quantitative Insights Into Microbial Ecology QIIME2 pipeline (v. 2023.7), 16S rRNA gene sequences were first demultiplexed and then quality trimmed based on the average quality per base of the forward and reverse reads. Consequently, reads were merged, and chimeric variants were removed. All amplicon sequence variants (ASVs) were aligned with MAFFT (Katoh, 2002) (using q2-alignment) and q2-phylogeny to construct a phylogeny with FastTree 2 (Price et al., 2010). Alpha and beta microbial diversity metrics were calculated using the q2-diversity plugin in QIIME2 (Bolyen et al., 2019). Taxonomic assignment to ASVs was accomplished using the Classify-Sklearn Naive Bayes method based on the 16S rRNA SILVA database v.138 (Yarza et al., 2014), trained 99 %, using the same primer used for sequencing. The resulting taxonomic data tables were collapsed at the genus level and taxa with $< 10$ total reads and present in $< 30$ % of samples of each dataset were removed. The taxonomic data tables were used for network analysis.

### 2.3. Comparison of microbial diversity indexes metrics and differential taxonomic composition

The alpha diversity metrics (i.e. Observed Features, Faith's Phylogenetic Diversity and Pielou's Evenness) (Bolyen et al., 2019; Faith, 1992; Pielou, 1966) were estimated to assess the within-sample diversity using the Kruskal-Wallis test ($p < 0.05$) in QIIME2 (Bolyen et al., 2019). Sampling depth was assessed by examining rarefaction curves based on a sub-sampling depth of 10,000 sequences per sample.

The calculation of the Jaccard coefficient of similarity and its representation as a cladogram was done using the "Vegan" package (Oksanen et al., 2020) implemented in RStudio (RStudio Team, 2020). Bacterial beta diversity was assessed using the Bray-Curtis dissimilarity index (Bray and Curtis, 1957) in QIIME 2 (Bolyen et al., 2019) and compared among groups using a PERMANOVA test ($p < 0.05$). Beta dispersion (variance) was calculated using the "betadisper" function and "Vegan" package implemented in RStudio (RStudio Team, 2020) and compared among groups using an ANOVA test ($p < 0.05$).

The number of shared or unique taxa among the different groups under study were visualized using Venn diagrams created with an online tool (http://bioinformatics.psb.ugent.be/webtools/Venn/).

The abundance of each microbial taxa was compared between the conditions. The data were transformed into centered log ratio (clr) values, utilizing the geometric mean of the read counts in each sample to assess relative abundance (Aitchison, 1982). The clr value transformation was performed with the 'ANOVA-like differential expression' ('ALDEx2') package (Fernandes et al., 2013) in the R program (v.4.1.2) (R Core Team, 2023). Only taxa with a significant corrected p-value ($p < 0.05$) were visualized as taxa with differential abundance. The resulting dataset was used to construct the heatmap with the "Heatplus" packages implemented in RStudio (RStudio Team, 2020).

### 2.4. Inference of bacterial co-occurrence networks

Co-occurrence networks were constructed as a graphical representation of the microbial community structures using taxonomic profiles. Networks were built using Sparse Correlations for Compositional Data (SparCC) method (Friedman and Alm, 2012) as implemented in the "SpiecEasi" package (Kurtz et al., 2015) in R (RStudio Team, 2020). Taxonomic data tables were used to calculate the correlation matrix. Correlation coefficients with magnitude $> 0.30$ or $< -0.30$ were selected. Network visualization and calculation of topological features and taxa connected (i.e. number of nodes and edges, modularity, network diameter, average degree, weighted degree, clustering coefficient, and centrality metrics) were performed using the software Gephi 0.9.2 (Bastian et al., 2009). Only significant correlations between taxa are represented by edges, with p-values determined by bootstrapping methods.

In addition, core association network (CAN) analysis was conducted with the Anuran software, implemented in Python 3.10. Anuran is a toolbox, designed to identify conserved patterns across networks. Its algorithm is based on a null models approach that generates random networks and assesses the properties of these networks, identifying non-random patterns in groups of networks using a core prevalence threshold of 0.8 (Röttjers et al., 2021).

### 2.5. Network comparisons

Network comparison was performed using the network construction and comparison for microbiome (NetCoMi) R package (Peschel et al., 2021). Positive (weight $\geq 0.30$) and negative (weight $\leq -0.30$) correlations were calculated without bootstrapping. To assess similarities in the distribution of local centrality measures across nodes (i.e., degree, betweenness centrality, closeness centrality and eigenvector centrality) between two networks, the Jaccard index was calculated for each centrality measure. In this context, the Jaccard index tests the similarity between sets of "most central nodes" (i.e., nodes with a centrality value above the empirical 75 % quartile) of two given networks, expressing the similarity of the most central nodes and hub taxa. Two p-values P ($J \leq j$) and P ($J \geq j$) were computed for each local centrality measure (Real and Vargas, 1996), for testing similarity in the distribution of local centrality measures between networks. The Jaccard index values of 0 and 1 represent minimum and maximum similarity, respectively (Real and Vargas, 1996).

### 2.6. Identification of keystone taxa

To determine keystone taxa, three criteria were employed. First, these taxa had to be ubiquitous, signifying that were present across all samples within a particular group. Second, their eigenvector centrality had to be higher than 0.75. Eigenvector centrality is a metric for measuring the influence of a node within a network. Third, the mean relative abundance of these taxa needed to exceed that of the mean relative abundance of all taxa in the experimental group (Mateos-Hernández et al., 2021). To conduct this analysis, eigenvector centrality values were extracted from Gephi 0.10 software. All taxa were plotted on a two-axis graph using Graphpad Prism, indicating the cutoff points for clr and eigenvector centrality.

### 2.7. Network robustness analysis

The proportion of node removal needed to reach a loss of 0.80 in the connectivity of each network was recorded using random or directed attack. Directed attacks are based on betweenness centrality (removing first node with the highest betweenness centrality values), degree (removing nodes with the highest degree centrality values), and cascading (removing first node with the highest betweenness centrality values with recalculation of betweenness centrality after removal of each node). The network robustness analysis was performed using Network Strengths and Weaknesses Analysis (NetSwan) package (Lhomme, 2015) in R (RStudio Team, 2020). Connectivity loss variability was assessed by calculating the standard error, using a threshold of 0.975.

To evaluate the specific contribution of *Staphylococcus* and the identified keystone taxa to network structure, we conducted an *in-silico* removal by deleting those taxa from the taxonomic table (for both water-treated and bleach-treated cohorts), reconstructed the corresponding depleted subgraphs, and repeated the full robustness workflow under degree-targeted, betweenness-targeted, and cascading attack schemes. Centrality rankings were recalculated on the depleted networks at each deletion step for each attack, and the proportion of nodes required to reach 0.80 connectivity loss was compared between original and taxa-depleted networks.

The statistical analysis used was a ANOVA followed by post hoc multiple-comparison tests and paired t-test, for all pairwise comparisons.

### 2.8. Assessment of Staphylococcusabundance and its potential role in Borreliacolonization

The relative abundance of *Staphylococcus* was compared across experimental conditions. To normalize the data, read counts were transformed using centered log-ratio (CLR) values, calculated based on the geometric mean of each sample (Aitchison, 1982). Group comparisons were performed using an unpaired *t*-test ($p < 0.05$) to assess differences in *Staphylococcus* abundance between conditions. To evaluate the relationship between *Borrelia* and *Staphylococcus*, CLR-transformed values were analyzed within permissive nymphs, the only group in which both taxa co-occurred across samples. Pearson correlation

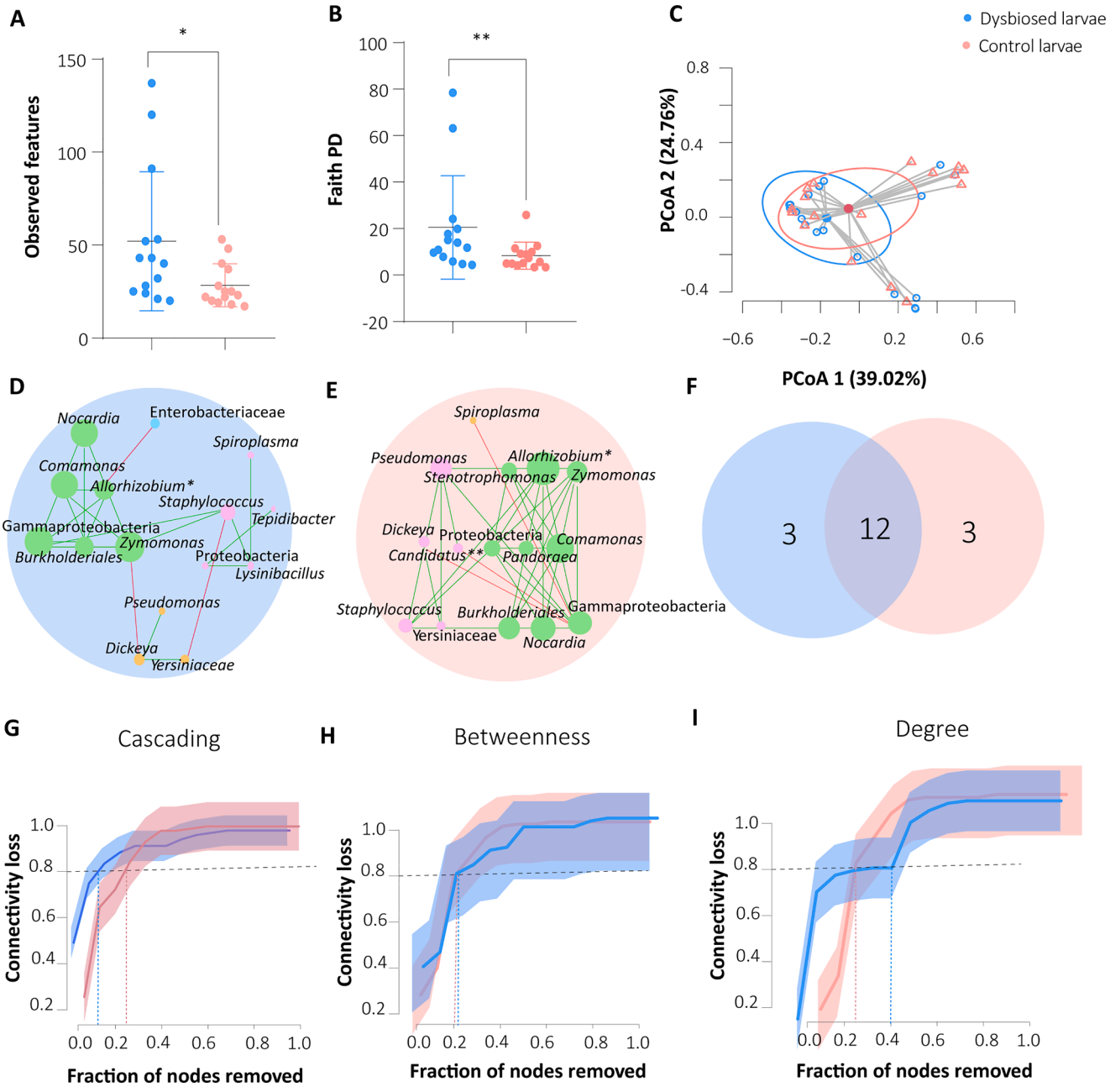


**Fig. 2.** Dysbiosis alters microbial diversity, community assembly, and robustness in *Ixodes ricinus* larvae. Alpha diversity was assessed using (A) Observed Features and (B) Faith's Phylogenetic Diversity, which revealed significantly higher richness and phylogenetic diversity in dysbiosed larvae compared to normal larvae (Kruskal–Wallis, $p = 0.036$ and $p = 0.006$, respectively). (C) Beta diversity was analyzed using Bray–Curtis dissimilarity to assess community composition differences between the two groups (PERMANOVA, $p = 0.331$). Symbols denote groups, triangles: normal larvae and circles: dysbiosed larvae. Ellipses indicate group centroids (dispersion shown around each centroid). Bacterial co-occurrence networks were inferred from 16S rRNA gene sequences obtained from (D) dysbiosed and (E) normal larvae. Networks were constructed based on SparCC correlations (SparCC > 0.30 or < 0.30). Nodes represent bacterial taxa, with size proportional to eigenvector centrality and color indicating modularity class. Edges represent negative (red) or positive (green) associations. Allorhizobium* denotes the *Allorhizobium-Neorhizobium-Pararhizobium-Rhizobium* complex and *Candidatus***denotes the *Candidatus* Midichloria. (F) Venn diagram showing the number of bacterial taxa shared or unique between dysbiosed and normal larvae networks. Network robustness was evaluated via node removal using three direct attack strategies: (G) cascading, (H) betweenness-based, and (I) degree-based attacks.

(one-tailed, $\alpha = 0.05$) was applied, and the correlation coefficient ($r$) and $p$-value were reported. All analyses and scatterplots of clr (*Staphylococcus*) and clr (*Borrelia*) were conducted in GraphPad Prism (v 8.0.1).

## 3. Results

### 3.1. Sequence analysis

We analysed tick bacterial microbiomes separately according to microbiome manipulation (dysbiosed larvae hatched from eggs rinsed with bleach versus control larvae hatched from eggs rinsed with water) and pathogen exposure (ticks fed on infected versus uninfected mice), including both tick stages. For water-treated tick raw data, DADA2 denoising retained an average of 45,779 non-chimeric, high-quality sequences per sample after quality filtering, merging, and chimera removal; 1192 amplicon sequence variants (ASVs) (90.56 % of original reads) remained after excluding eukaryotic, mitochondrial, and taxonomically unassigned sequences, with >98 % of ASVs 130 nucleotides long, and genus-level profiling resolved 43 taxa. For bleached tick raw data, DADA2 retained an average of 39,688 such sequences per sample (91.81 % of original reads); 1610 ASVs remained after the same exclusions, with >98 % 130 nucleotides long, and genus-level profiling resolved 39 taxa.

### 3.2. Dysbiosis alters microbial community structure and weakens network robustness in I. ricinus larvae

*Ixodes ricinus* larvae hatched from the surface-sterilized eggs (dysbiosed larvae) were compared to that of *I. ricinus* control eggs (control larvae). Hamilton et al. (2021) showed that egg bleaching modifies the microbial composition of I. ricinus larvae. Building on this, we employed a network-based approach to investigate how dysbiosis influences microbial community assembly in larvae.

Alpha diversity analyses revealed that dysbiosed larvae harbored significantly higher microbial richness and phylogenetic diversity than control larvae, as indicated by increased observed features ($p = 0.036$, Fig. 2A) and Faith's Phylogenetic Diversity ($p = 0.006$, Fig. 2B). No significant differences were observed in Pielou's evenness between the dysbiosed larvae and control larvae ($p = 0.408$, Supplementary Fig. S1A), indicating that community uniformity remained stable despite changes in richness. Beta diversity analysis based on Bray-Curtis dissimilarity did not reveal statistically significant compositional differences between dysbiosed larvae and control larvae (PERMANOVA, $p = 0.331$), and no significant differences in dispersion were detected (ANOVA, $p = 0.435$, Fig. 2C). To complement diversity metrics, we next examined microbial co-occurrence networks to gain insight into community assembly and taxa interactions.

Network analysis revealed a pronounced reduction in structural connectivity in dysbiosed larvae (Fig. 2D), characterized by fewer edges, lower average and weighted degree, and decreased clustering coefficient compared to normal larvae (Fig. 2E, Table 1), suggesting a less cohesive and potentially destabilized microbial community. Positive associations predominated in both groups (Fig. 2D-E, Table 1). Comparison of node identity showed shared taxa such as *Pseudomonas, Staphylococcus, Nocardia* and taxa exclusive to the network of control larvae (e.g. *Pandoraea, Stenotrophomonas* and *Candidatus* Midichloria) and dysbiosed larvae network (e.g. Enterobacteriaceae, Lysinibacillus and Tepidibacter) (Fig. 2F, Supplementary Table S1).

To better understand how these changes in the topological features of the network affect the role of individual taxa within the community, Jaccard similarity index analysis was performed to evaluate the differences in local centrality measures between the networks. Closeness centrality ($P(\geq Jacc) = 0.045$) and eigenvector centrality ($P(\geq Jacc) = 0.045$) were significantly higher than expected by random, indicating non-random reallocation of central roles across networks (Table 2).

In the network of dysbiosed larvae (Supplementary Fig. S1B), taxa such as *Burkholderiales, Staphylococcus, Lysinibacillus, Proteobacteria,* and Gammaproteobacteria exhibited increased closeness centrality compared to the network of normal larvae (Supplementary Fig. S1C), reflecting a more central topological position and shorter path distances to other taxa within the microbial association network. Similarly, *Burkholderiales, Staphylococcus, Comamonas, Nocardia*, and *Allorhizobium-Neorhizobium-Pararhizobium-Rhizobium* displayed higher eigenvector centrality in dysbiosed larvae network.

One crucial aspect of networks is their ability to withstand perturbations such as the removal of nodes. Among the different attack strategies tested, direct (targeted) attacks had the most pronounced effect on network integrity (Fig. 2G–I), while random node removal was the least disruptive across all conditions (Supplementary Fig. S1D). Under cascading attack, the dysbiosed larvae network lost 80 % of its connectivity after the removal of just 13 % of nodes, whereas the control larvae network required the removal of 26 % of nodes to reach the same level of disconnection (Fig. 2G). Betweenness-based attack, both dysbiosed and control larvae networks reached 80 % connectivity loss after the removal of 20 % of nodes (Fig. 2H). Degree-based attack produced opposite results: dysbiosed larvae networks required the removal of 40 % of nodes, while control larvae reached the same loss with only 26 % removed (Fig. 2I), implying that hubs in the dysbiosed network may be less influential or less interconnected. Finally, under random removal, dysbiosed larvae lost 80 % of connectivity after removing 40 % of nodes, while control larvae required 46 % of node removal (Supplementary Fig. S1D). Statistical comparisons of robustness curves indicated that none of the observed differences between dysbiosed and control larval networks across directed attack strategies were statistically significant (Supplementary Table S2).

### 3.3. Dysbiosis status shapes microbial diversity in Borrelia-permissive and refractory nymphs

To evaluate how pathogen exposure and microbiome manipulation influence microbiota composition in *I. ricinus* nymphs, we analyzed individuals originating from larvae with or without dysbiosis that were fed on either *B. afzelii*–infected or uninfected mice. This generated six experimental groups: control-normal nymphs (CN), derived from control larvae fed on uninfected mice; permissive-normal nymphs (PN), derived from control larvae fed on infected mice and successfully

**Table 1**
Topological features of normal and dysbiosed larvae networks.

| Topological features | Normal larvae | Dysbiosed larvae |
|---|---|---|
| Nodes | 15 | 15 |
| Edges | 43 | 26 |
| Positive | 40 (93.03 %) | 23 (88.46 %) |
| Negative | 3 (6.97 %) | 3 (11.54 %) |
| Modularity | 0.16 | 0.36 |
| Network diameter | 3 | 6 |
| Average degree | 5.73 | 3.46 |
| Weighted degree | 2.90 | 1.49 |
| Clustering coefficient | 0.82 | 0.46 |
| Number of communities | 3 | 4 |

**Table 2**
Jaccard index for normal and dysbiosed larvae networks.

| Parameters | Normal larvae vs Dysbiosed larvae | | |
|---|---|---|---|
| | J | P(≤Jacc) | P(≥Jacc) |
| Degree | 0.667 | 0.982 | 0.100 |
| Betweenness centrality | 0.167 | 0.351 | 0.912 |
| Closeness centrality | 0.714 | 0.993 | 0.045* |
| Eigenvector centrality | 0.714 | 0.993 | 0.045* |
| Hub taxa | 0.500 | 0.888 | 0.407 |

Significance codes:.
*: 0.05.

colonized by *B. afzelii*; refractory-normal nymphs (RN), from control larvae fed on infected mice but not colonized; control-dysbiosed nymphs (CD), from dysbiosed larvae fed on uninfected mice; permissive-dysbiosed nymphs (PD), from dysbiosed larvae fed on infected mice and colonized; and refractory-dysbiosed nymphs (RD), from dysbiosed larvae fed on infected mice and not colonized. This experimental design allowed us to compare microbiota features of *I. ricinus* nymphs as a function of larval dysbiosis, *B. afzelii* exposure, and *B. afzelii* colonization outcome.

The transition from larvae to nymphs was associated with a significant increase in microbiota diversity, as measured by Pielou's evenness, Observed features, and Faith's phylogenetic diversity (Supplementary Table S3). Compared to control larvae, control-normal nymphs, permissive-normal nymphs and refractory-normal nymphs displayed significantly higher values across all three metrics, indicating an expansion and homogenization of the microbial community (Supplementary Table S3). In the cases of dysbiosed ticks, only for Pielou's evenness, permissive-dysbiosed nymphs and refractory-dysbiosed nymphs, displayed significantly higher values dysbiosed-larvae (Supplementary Table S3).

Among normal nymphs, permissive-normal nymphs had significantly higher values than control-normal nymphs across all metrics (Fig.3A, Supplementary Table S3). Pielou's evenness was the only metric significantly higher in refractory-normal nymphs compared to control-normal nymphs (Fig.3A, Supplementary Table S3). No significant differences were identified between permissive and refractory normal nymphs (Fig. 3A, Supplementary Table S3). For the nymphs resulting from dysbiosed larvae, only for Faith's phylogenetic diversity, we identified a significant increase of the diversity of permissive-dysbiosed nymphs compared to control-dysbiosed nymphs (Fig. 3B, Supplementary Table S3).

Beta diversity analysis revealed significant differences in microbial community composition between larvae and the resultant nymphs, under both control (Fig. 3C) and dysbiosed conditions (Fig. 3D, Supplementary Table S4). Within the nymphal stage, beta diversity significantly differed between control nymphs and nymphs that fed on *B. afzelii*-infected mice, regardless of whether they originated from normal or dysbiosed larvae (Fig. 3C–D, Supplementary Table S4). However, no significant differences were found between permissive and refractory nymphs under microbiome manipulation (Fig. 3C–D, Supplementary Table S4).

Taxonomic composition analysis revealed that 50 % of the detected taxa (21 out of 42) were shared across all six types of nymphs, supporting the presence of a shared microbiota. Shared taxa included *Allorhizobium–Neorhizobium–Pararhizobium–Rhizobium, Spiroplasma, Nocardia, Candidatus* Midichloria, and *Staphylococcus*. In addition to this shared core, group-specific taxa also emerged, highlighting compositional shifts associated with microbiome manipulation and pathogen exposure (Fig. 3E, Supplementary Table S5).

### 3.4. *Dysbiosis and pathogen exposure drive network destabilization in permissive nymphs and structural resilience in refractory ones*

To further investigate the mechanisms underlying colonization resistance, we next examined microbial community assembly patterns in permissive and refractory nymphs. Using co-occurrence network approaches, we assessed whether differences in taxa interactions, centrality, and network topology could reveal functional features of the microbiota linked to resistance or susceptibility.

In terms of community assembly, refractory-normal nymphs (Fig. 4A) exhibited greater network complexity than permissive-normal nymphs (Fig. 4B), with higher numbers of nodes, edges, modularity, average degree, and communities (Table 3). Both refractory-normal and permissive-normal nymphs also showed more complex networks than control-normal nymphs (Fig. 4C, Table 3). Core associations were consistently observed between Alphaproteobacteria and *Candidatus* Midichloria, as well as between *Nocardia* and *Mycobacterium* (Supplementary Fig. S2A).

Among dysbiosed nymphs, refractory-dysbiosed nymphs (Fig. 4D) exhibited the highest structural complexity, characterized by greater

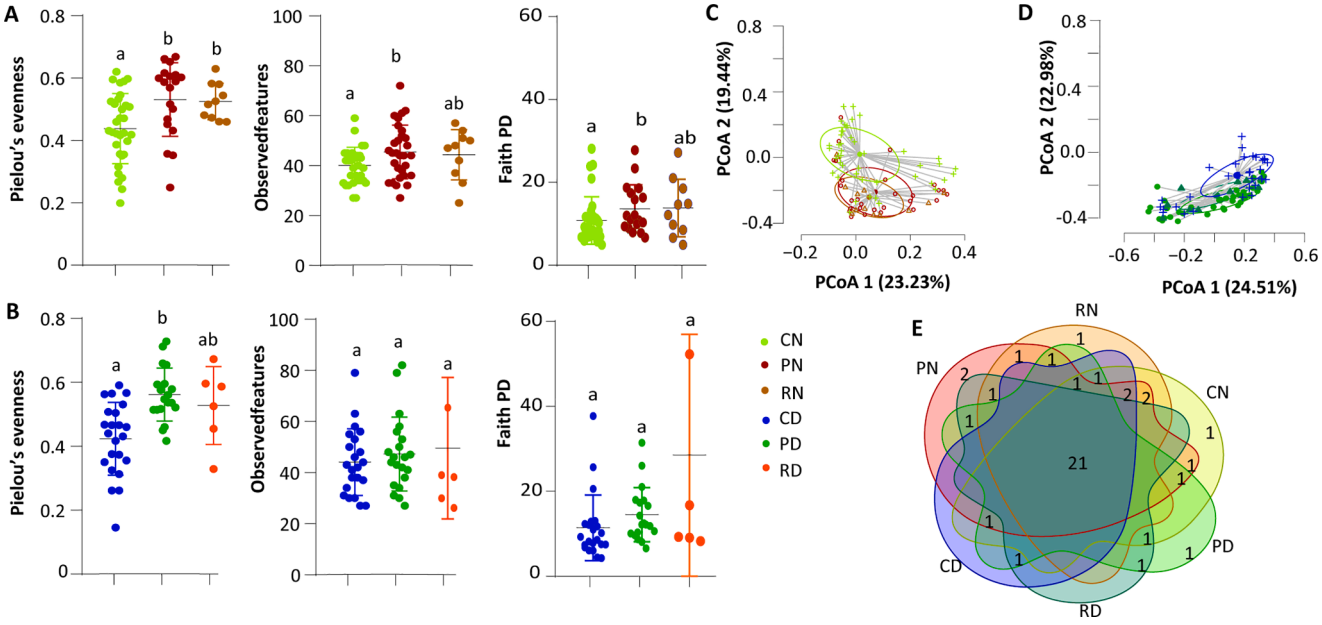


**Fig. 3.** Alpha and beta diversity metrics and shared taxa across nymph groups. Alpha diversity was assessed using: Pielou's evenness, Observed features, and Faith's phylogenetic diversity for nymphs resulting from larvae resulting of eggs treated with (A) water or (B) bleach. Significant differences in alpha diversity between groups were determined using Kruskal-Wallis test. Different lowercase letters indicate significant differences ($p < 0.05$). Principal Coordinates Analysis (PCoA) based on Bray-Curtis showing beta diversity among control (C: CN vs RN vs PN) and dysbiosed (D: CD vs RD vs PD) nymphs. Ellipses represent 95 % confidence intervals for each group. (E) Venn diagram showing the number of shared and unique taxa among the six nymphal groups: control-normal (CN), permissive-normal (PN), refractory-normal (RN), control-dysbiosed (CD), permissive-dysbiosed (PD), and refractory-dysbiosed (RD). The central intersection indicates the core microbiota shared across all groups.

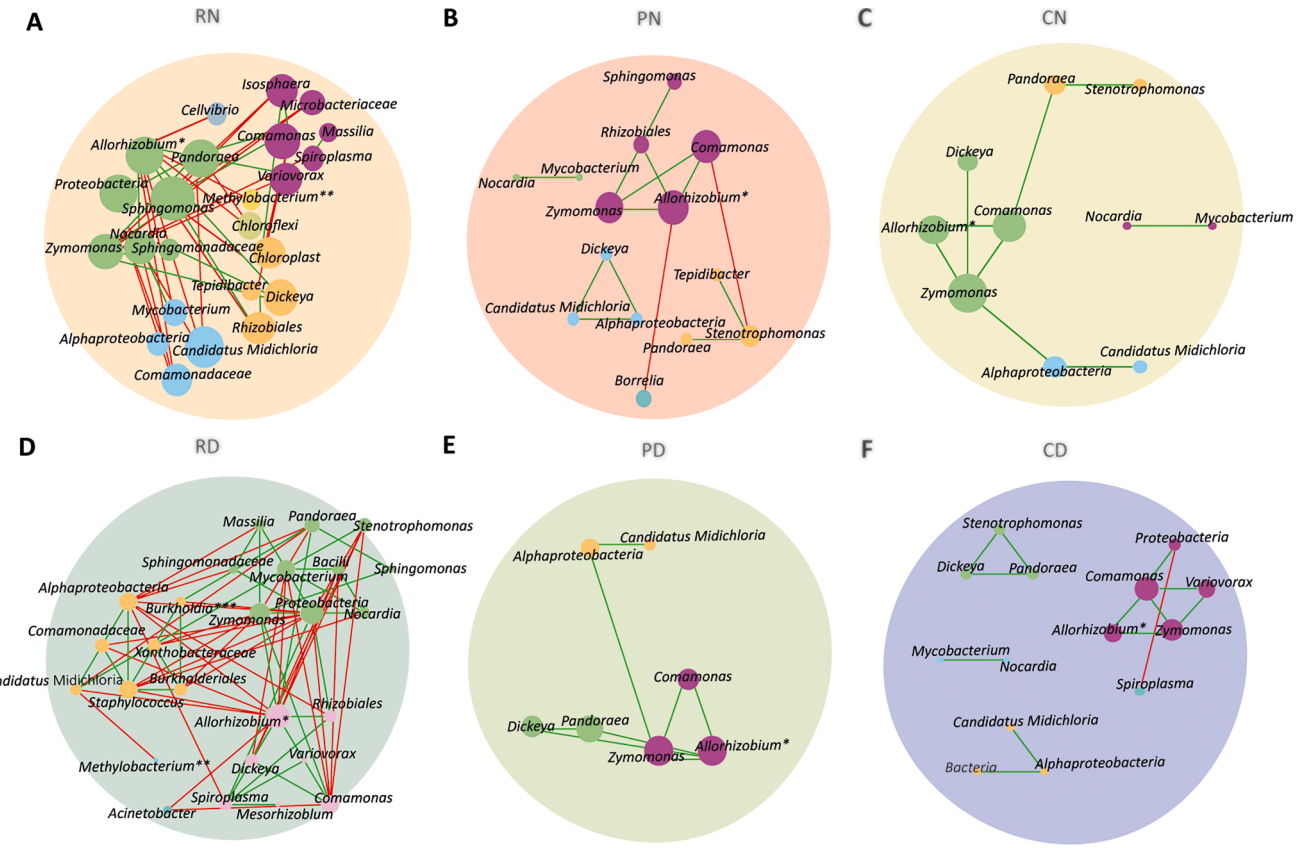


**Fig. 4.** Microbial co-occurrence networks in *Ixodes ricinus* nymphs. Co-occurrence networks were inferred from 16S rRNA gene sequences using SparCC correlations (SparCC $>$ 0.30 or $<$ 0.30). Nodes represent bacterial taxa; edges indicate negative (red) or positive (green) associations. Node size is proportional to eigenvector centrality, and node color indicates modularity class. Networks are shown for (A) refractory-normal (RN), (B) permissive-normal (PN), (C) control-normal (CN), (D) refractory-dysbiosed (RD), (E) permissive-dysbiosed (PD), and (F) control-dysbiosed (CD) nymphs. Asterisks (*) denote the *Allorhizobium-Neorhizobium-Pararhizobium-Rhizobium* complex. Taxa labels correspond to the genus level or higher taxonomic ranks when genus-level assignment was not available.

**Table 3**
Topological features of nymphs network.

| Topological features | CN | PN | RN | CD | PD | RD |
|---|---|---|---|---|---|---|
| Nodes | 10 | 14 | 24 | 12 | 7 | 26 |
| Edges | 9 | 13 | 54 | 11 | 8 | 73 |
| Positive | 9 (100 %) | 11 (84,6 %) | 32 (59,25 %) | 11 (100 %) | 8 (100 %) | 37 (50,68 %) |
| Negative | - | 2 (15,4 %) | 22 (40,74 %) | - | - | 36 (49,31 %) |
| Modularity | 0.44 | 0.78 | 1.81 | 0.61 | 0.24 | 5.90 |
| Network diameter | 5 | 4 | 4 | 2 | 4 | 4 |
| Average degree | 1.80 | 1.85 | 4.50 | 1.83 | 2.28 | 5.61 |
| Weighted degree | 0.95 | 0.62 | 0.34 | 0.89 | 1.14 | 0.13 |
| Clustering coefficient | 0.3 | 0.54 | 0.55 | 0.85 | 0.61 | 0.58 |
| Number of communities | 4 | 5 | 7 | 4 | 3 | 5 |

connectivity and modular organization compared to both permissive-dysbiosed (Fig. 4E) and control-dysbiosed nymphs (Fig. 4F, Table 3). In contrast, permissive-dysbiosed nymphs (Fig. 4E) showed a marked loss of structural organization, characterized by fewer nodes and edges, lower modularity, and the absence of negative correlations (Table 3). Notably, control-dysbiosed nymphs retained greater network complexity than permissive-dysbiosed nymphs. Core associations in dysbiosed networks prominently involved *Mycobacterium, Comamonas,* and *Zymomonas,* suggesting persistent microbial interactions despite the altered community context (Supplementary Fig. S2B).

Control-dysbiosed nymphs (Fig. 4F) exhibited greater network complexity than control-normal nymphs (Fig. 4C), with higher numbers of nodes, edges, modularity, average degree, and clustering coefficient (Table 3). In contrast, permissive-dysbiosed nymphs (Fig. 4E) showed a marked reduction in network complexity compared to their normal counterparts (Fig. 4B), with fewer nodes and edges, lower modularity, and a reduced number of communities (Table 3). Notably, only positive associations were detected in permissive-dysbiosed networks, whereas both positive and negative correlations were present in permissive-normal networks (Table 3). Refractory-dysbiosed nymphs (Fig. 4D), on the other hand, exhibited higher complexity than refractory-normal nymphs (Fig. 4A), with increased numbers of nodes, edges, negative associations, modularity, average degree, and clustering coefficient (Table 3). Importantly, no shared core associations were detected across all groups, indicating that the dysbiosis condition reshaped network community and disrupted conserved microbial interaction patterns.

To gain deeper insights into the reorganization of community assembly across microbial networks, we analyzed the similarity of central taxa using the Jaccard similarity index. No significant deviations from random expectations were observed between control-normal and refractory-normal nymph networks across any centrality metric (Table 4), indicating a largely conserved network structure. In contrast, between control-normal and permissive-normal nymphs, closeness centrality showed a significantly higher similarity than expected by random ($P(\geq Jacc) = 0.045$, Table 4), suggesting partial overlap in the nodes occupying central network positions. Meanwhile, the comparison between refractory-normal and permissive-normal nymphs revealed

**Table 4**
Jaccard index for control-normal nymphs, refractory-normal nymph and permissive-normal nymph networks.

| Parameters | CN vs RN | | | CN vs PN | | | PN vs RN | | |
|---|---|---|---|---|---|---|---|---|---|
| | J | P(≤Jacc) | P(≥Jacc) | J | P(≤Jacc) | P(≥Jacc) | J | P(≤Jacc) | P(≥Jacc) |
| Degree | 0.571 | 0.954 | 0.173 | 0.333 | 0.650 | 0.622 | 0.273 | 0.472 | 0.765 |
| Betweenness centrality | 0.571 | 0.954 | 0.173 | 0.250 | 0.468 | 0.804 | 0.077 | 0.038* | 0.994 |
| Closeness centrality | 0.400 | 0.786 | 0.440 | 0.714 | 0.993 | 0.045* | 0.167 | 0.181 | 0.946 |
| Eigenvector centrality | 0.400 | 0.786 | 0.440 | 0.333 | 0.650 | 0.622 | 0.167 | 0.181 | 0.946 |
| Hub taxa | 0.200 | 0.460 | 0.868 | 0.500 | 0.888 | 0.407 | 0.000 | 0.087. | 1.000 |

Significance codes:.
* : 0.05,¨: 0.1.

significantly lower-than-expected similarity in betweenness centrality (P(≤Jacc) = 0.038, Table 4) and a marginal deviation for hub taxa (P (≤Jacc) = 0.088, Table 4), pointing to a structural reconfiguration of key microbial connectors associated with *Borrelia* colonization.

Control-dysbiosed nymphs exhibited a higher number of hub taxa than both refractory-dysbiosed (*P*(≥Jacc) = 0.010) and permissive-dysbiosed nymphs (*P*(≥Jacc) = 0.088), indicating a reduction in network centrality with increased susceptibility (Table 5). When comparing refractory-dysbiosed and permissive-dysbiosed nymphs, a non-random overlap was observed in degree (P(≥Jacc) = 0.076), closeness centrality (P(≥Jacc) = 0.039), and eigenvector centrality (P (≥Jacc) = 0.003), suggesting shared influential taxa despite differing infection outcomes (Table 5). However, similarities in betweenness and hub taxa did not differ from random expectations, highlighting a selective retention of specific network roles rather than a generalized structural conservation.

Regardless of the microbiome manipulation (normal and dysbiosed), refractory nymphs consistently exhibited networks enriched in highly connected and structurally influential taxa compared to permissive nymphs. *Allorhizobium–Neorhizobium–Pararhizobium–Rhizobium* and *Gammaproteobacteria* were central in refractory-normal nymph networks across degree, betweenness centrality and closeness centrality metrics, whereas these taxa lost nearly all centrality in permissive-normal nymphs (Supplementary Fig. S3). A similar pattern was observed under dysbiosis, where *Allorhizobium–Neorhizobium –Pararhizobium–Rhizobium* and *Proteobacteria* retained high degree and betweenness centrality in refractory-dysbiosed nymphs but markedly declined in permissive-dysbiosed networks (Supplementary Fig. S4). *Staphylococcus* emerged as a structurally relevant taxon exclusively in refractory networks, both normal and dysbiosed, where it displayed elevated degree and closeness centrality (Supplementary Fig. S3–4). Notably, *Spiroplasma* and *Mycobacterium* became central in refractory-dysbiosed nymphs across multiple centrality measures, further reinforcing the association between network cohesion and infection resistance. Altogether, taxa like *Allorhizobium–Rhizobium, Proteobacteria, Spiroplasma*, and *Staphylococcus* appear as consistent structural hubs in refractory networks, while their loss of centrality in permissive counterparts reflects a weakened and less integrated microbial community architecture.

Statistical analyses revealed no significant differences in network robustness between permissive-normal (PN) and refractory-normal (RN) nymphs under any of the direct attack strategies tested (Fig. 5A–C, Supplementary Table S6, Supplementary Fig. S5 A-C). In contrast, when compared with control nymph (CN) networks, both PN and RN networks exhibited significantly increased robustness across all direct attack strategies (Fig. 5A–C, Supplementary Table S6). Notably, relative to larval networks (LN), a significant increase in robustness was detected only in RN nymph networks (Fig. 5A–C, Supplementary Table S6).

Under dysbiosed conditions, statistical comparisons indicated that permissive-dysbiosed (PD) networks were significantly less robust than refractory-dysbiosed (RD) networks only under cascading attack (Fig. 5D, Supplementary Table S6, Supplementary Fig. S5 A-C). No significant differences between PD and RD networks were observed under the remaining attack strategies (Fig. 5E–F, Supplementary Table S6). Compared with control-dysbiosed (CD) nymph networks, RD networks showed significantly increased robustness under cascading and degree-based attacks (Fig. 5D,5F, Supplementary Table S6), whereas PD networks exhibited a significant increase only under degree-based attacks (Fig. 5F, Supplementary Table S6). Furthermore, relative to larval-dysbiosed networks (LD), both PD and RD nymph networks displayed significantly higher robustness under cascading and degree-based attacks; however, under betweenness-based attacks, a significant increase was observed exclusively in RD networks (Fig. 5D–F, Supplementary Table S6).

### 3.5. Role of staphylococcuson microbiota integrity

Building on the observation that *Staphylococcus* consistently emerged as a structurally central taxon, particularly in refractory-nymph networks, we further investigated the ecological role of *Staphylococcus* in shaping community architecture and potentially mediating resistance to *Borrelia afzelii*.

*Staphylococcus* was presents in all the tick groups (Supplementary Table S7). Notably, the relative abundance of *Staphylococcus* was significantly higher in dysbiosed larvae ($p$ = 0.0075), permissive-dysbiosed nymphs ($p$ = 0.002), and refractory-dysbiosed nymphs ($p$ = 0.04) compared with their corresponding normal tick groups (Fig. 6A). These results prompted us to explore whether *Staphylococcus* co-varies with *Borrelia* in groups susceptible to infection. A Pearson correlation analysis revealed a positive association between *Borrelia* and *Staphylococcus* CLR values in permissive-normal nymphs ($r$ = 0.6266, $p$ = 0.0007; Fig. 6B) and permissive-dysbiosed nymphs ($r$ = 0.5242, $p$ =

**Table 5**
Jaccard index dysbiosed larvae vs control-dysbiosed, refractory-dysbisoed nymphs and permissive-dysbisoed nymphs networks.

| Parameters | CD vs RD | | | CD vs PD | | | PD vs RD | | |
|---|---|---|---|---|---|---|---|---|---|
| | J | P(≤Jacc) | P(≥Jacc) | J | P(≤Jacc) | P(≥Jacc) | J | P(≤Jacc) | P(≥Jacc) |
| Degree | 0.429 | 0.826 | 0.429 | 0.444 | 0.855 | 0.349 | 0.600 | 0.980 | 0.076. |
| Betweenness centrality | 0.400 | 0.786 | 0.440 | 0.667 | 0.982 | 0.100 | 0.400 | 0.786 | 0.440 |
| Closeness centrality | 0.385 | 0.758 | 0.447 | 0.385 | 0.758 | 0.447 | 0.636 | 0.991 | 0.038* |
| Eigenvector centrality | 0.500 | 0.933 | 0.177 | 0.385 | 0.758 | 0.447 | 0.800 | 0.999 | 0.003** |
| Hub taxa | 0.583 | 0.996 | 0.010* | 0.533 | 0.969 | 0.088. | 0.417 | 0.859 | 0.253 |

Significance codes:.
** : 0.01,.
* : 0.05 ,¨: 0.1.

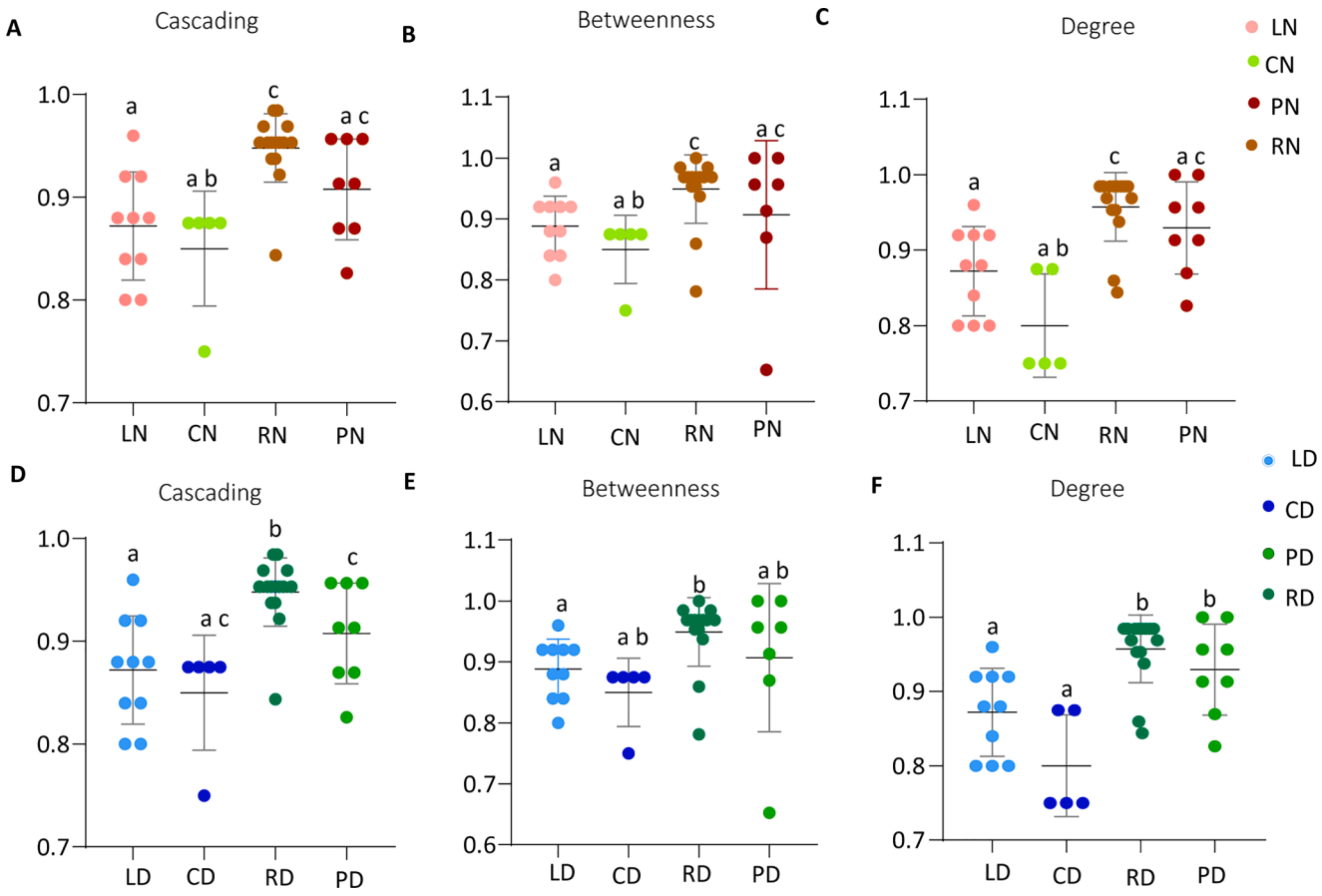


**Fig. 5.** Comparison of network robustness to taxa removal across tick developmental stages and microbiome treatments. Robustness was evaluated for microbial association networks constructed from larval and nymphal stages under control (water-treated) and dysbiosed (bleach-treated) conditions. Sequential node removal was applied using three targeted attack strategies: cascading, betweenness-based, and degree-based, to non-dysbiosed (A–C) and dysbiosed (D–F) networks. Robustness was quantified as the proportion of nodes removed to reach a defined threshold of network connectivity loss and is presented on a normalized scale ranging from 0 (fully connected network) to 1 (complete network disconnection). Different letters indicate statistically significant differences among groups, whereas shared letters indicate no significant differences, based on *t*-test.

0.0012; Fig. 6C). These findings point to two non-exclusive hypotheses in susceptible ticks: first, that increased Staphylococcus abundance co-occurs with microbiota configurations that are permissive to Borrelia colonization; and second, that Borrelia acquisition during the larval blood meal may be associated with subsequent Staphylococcus colonization of the tick microbiota.

To better understand the potential role of *Staphylococcus* in maintaining community integrity, we examined its direct associations within the co-occurrence networks. In the co-occurrence networks of both permissive-normal and permissive-dysbiosed nymphs, we did not detect any direct or indirect interaction between *Borrelia* and *Staphylococcus*. In refractory-dysbiosed nymphs, *Staphylococcus* exhibited negative associations with *Allorhizobium–Neorhizobium–Pararhizobium–Rhizobium* and *Zymomonas*, two nodes identified as keystone taxa in the network (Supplementary Fig. S6). Interestingly, in permissive-normal nymphs, *Borrelia* was also negatively associated with the keystone taxon *Allorhizobium–Neorhizobium–Pararhizobium–Rhizobium*.

These patterns prompted us to evaluate how the removal of *Staphylococcus* (woSta) or *Allorhizobium–Neorhizobium–Pararhizobium–Rhizobium* (wokeystone), a keystone taxon, would affect overall network structure. In control-normal nymph networks, targeted removal of either *Staphylococcus* or the keystone taxon did not result in statistically significant changes in robustness compared with the intact network (Supplementary Fig. S7A). In contrast, in control-dysbiosed nymph networks, *Staphylococcus* displayed a stronger association with network robustness, as its targeted removal led to a significant increase in robustness under betweenness-based ($p = 0.005$) and cascading ($p = 0.005$) attack strategies (Supplementary Fig. S8A). In refractory-normal (Fig. 6D) and refractory-dysbiosed (Fig. 6E) networks, *in silico* removal of *Staphylococcus* or, alternatively, removal of the keystone taxon did not produce statistically significant changes in robustness across attack strategies (Supplementary Fig. S7B; Supplementary Fig. S8B). In permissive-normal networks (Fig. 6F), removal of *Staphylococcus* produced significant decreases of the robustness under degree ($p = 0.048$) and betweenness ($p = 0.038$) attack, whereas keystone removal reached significance reductions under betweenness ($p = 0.0001$) and cascading ($p = 0.0001$) attacks (Supplementary Fig. S7C). In permissive-dysbiosed networks, none of the removal scenarios resulted in statistically significant robustness changes (Supplementary Fig. S8C).

## 4. Discussion

This study aimed to understand how microbial community structure and interactions are associated with *Borrelia afzelii* colonization outcomes in *Ixodes ricinus* ticks. In this study, we build on the work of (Hamilton et al., 2021), who tested the effects of manipulating the larval microbiome via egg bleaching on vector competence of immature *I. ricinus* for *B. afzelii*. Disruption of the larval microbiome largely disappears after larva-to-nymph molt and does not affect *B. afzelii* acquisition, as measured in the nymphal stage. Ethanol rinsing of nymphs produced only minor, context-dependent shifts in bacterial community and composition. By contrast, the larva-to-nymph transition

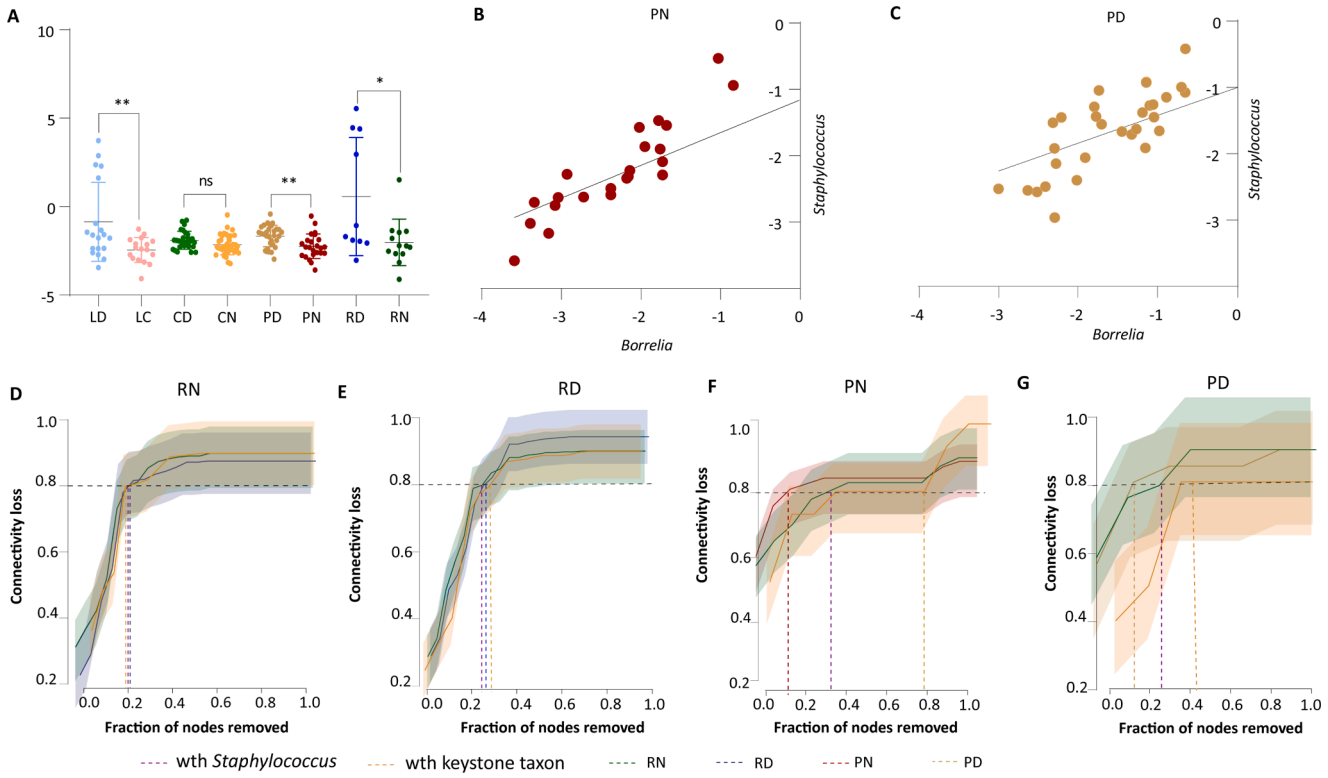


**Fig. 6.** *Staphylococcus* abundance, correlation with *Borrelia*, and impact on microbiota robustness in *Ixodes ricinus*. (A) Relative abundance of *Staphylococcus* (CLR-transformed) across all experimental groups, showing significantly higher levels in dysbiosed larvae (LD), permissive nymphs (PD), and refractory nymphs (RD) compared to their non-dysbiosed counterparts (Kruskal–Wallis, $p < 0.05$). Pearson correlation between *Borrelia* and *Staphylococcus* CLR values in (B) permissive-normal (PN) and (C) permissive-dysbiosed (PD) nymphs, revealing a significant positive association in both groups (PN: $r = 0.6266$, $p = 0.0007$; PD: $r = 0.5242$, $p = 0.0012$). Robustness analysis of microbial co-occurrence networks under degree-based node removal. Connectivity loss was plotted as a function of the fraction of nodes removed for (D) refractory-normal (RN), (E) refractory-dysbiosed (RD), (F) permissive-normal (PN), and (G) permissive-dysbiosed (PD) networks. In each panel, the effect of removing *Staphylococcus* (purple line) or a connected keystone taxon (orange line) is compared to total network robustness.

significantly reshapes the microbiota, with nymphs displaying increased diversity and pronounced shifts in the identity and relative abundance of dominant taxa compared to unfed larvae. Most notably, the infection status of the rodent host during the larval blood meal emerged as the primary driver of nymphal microbiome composition, more influential than the tick's own infection status. The study by Hamilton et al. (2021) supported a model were tick stage and host infection status determine microbial composition, while *Borrelia* exposure triggers more specific compositional tweaks rather than wholesale restructuring.

Yet, not all larvae that fed on infected mice developed into *B. afzelii*-positive nymphs, regardless of the egg microbiome manipulation (bleach or water). A straightforward explanation could be localized exposure variability, e.g., low or patchy spirochete presence at the bite site, consistent with the known tissue tropism of *B. afzelii* and the possibility that dorsal skin harbors lower loads than other tissues (Genné et al., 2021). However, Hamilton et al. (2021) used strain NE4049, which is highly infectious in both mice and ticks (Genné et al., 2019, 2018, 2021; Jacquet et al., 2016) making uneven exposure an unlikely sole explanation. Similar mismatches between exposure and infection have been observed in other systems, such as *Rhipicephalus microplus* feeding on *Anaplasma marginale*-infected cattle (Abuin-Denis et al., 2024a; Piloto-Sardiñas et al., 2024) or *I. ricinus* feeding on *Borrelia*-exposed birds (Heylen et al., 2015). This suggests that the divergence between permissive and refractory outcomes may depend not just on microbial diversity, but on the structural organization of the microbiome rather than diversity alone.

To build on the findings of Hamilton et al. (2021), we expanded both the analytical framework and the resolution of the data. Conceptually, we moved beyond a binary classification of exposure by introducing a three-tiered outcome comparison: unexposed controls, permissive ticks (exposed, *B. afzelii* positive), and refractory ticks (exposed, *B. afzelii* negative). This allowed us to explicitly dissect divergent outcomes following equivalent pathogen exposure. Methodologically, we shifted focus from community composition alone to network-level properties of microbial organization. By inferring association networks, we quantified key ecological features such as centrality (degree, betweenness), modularity, and system robustness under simulated perturbation (directed attacks, *in silico* removals), metrics that speak to community assembly and potential resistance to colonization.

To establish a pre-infection baseline, we characterized the microbiota of unfed larvae. This allowed us to capture the community prior to any blood meal-mediated shifts, providing a robust reference point for characterizing microbial state transitions associated with pathogen acquisition. In addition, we only included samples from ticks that underwent ethanol rinsing before DNA extraction. This decision is supported by prior microbiota work (Zolnik et al., 2016; Kwan et al., 2017) showing that ethanol rinsing reduces external contaminants while retaining internal and cuticle-associated microbes, increasing the confidence that detected taxa represent biologically relevant communities rather than environmental noise.

Critically, our approach re-analyzed the original Hamilton et al. (2021) dataset using updated bioinformatic pipelines and taxonomic references, thereby substantially improving taxonomic resolution and reproducibility. While the original study clustered sequences into OTUs using CD-HIT-OTU and annotated taxa via SILVA 132, we employed QIIME 2 with DADA2 to resolve amplicon sequence variants (ASVs), and classified them using the updated SILVA 138 database. This ASV-based approach enables single-nucleotide resolution, allowing for the detection of rare and low-abundance taxa that OTU clustering may obscure (Callahan et al., 2017; Nearing et al., 2022). Moreover, SILVA 138 offers

improved annotation coverage, particularly for uncultured or environmental taxa (Quast et al., 2013), which may explain the emergence of genera absent from the original publication. Together, these methodological advances reflect current best practices (Knight et al., 2018; Prodan et al., 2020) and enhance both the granularity and biological interpretability of the microbiome data.

Consistent with the original study, we found that larval feeding on mice significantly altered microbiota diversity in resultant nymphs. However, our findings further demonstrate that changes in diversity alone are insufficient to distinguish between permissive and refractory nymphs, suggesting that other factors, such as microbial community structure and network organization, play a more decisive role in shaping pathogen colonization outcomes. Similar results were observed in a study on *A. phagocytophilum* infection in *I. scapularis* ticks where no significant differences were observed in any metrics of alpha diversity but network assembly was reshaped after the infection (Abuin-Denis et al., 2024b).

Network analyses revealed that refractory nymphs harboured microbial communities with higher connectivity and increased modularity. These patterns are consistent with the hypothesis that structurally cohesive microbiomes may be associated with reduced *B. afzelii* establishment. This is in agreement with previous studies where microbial interaction, characterized by network structure rather than diversity, played a critical role in pathogen persistence in ticks (Abuin-Denis et al., 2024b), bird (Aželytė et al., 2024), and bee (Skičková et al., 2024). The increased clustering coefficient and connectivity observed in refractory nymphs suggest that greater network stability may be linked to reduced *Borrelia* establishment, potentially through competitive interactions, immune modulation, or microbiota-mediated metabolic constraints. An alternative and non-exclusive explanation is that these network properties represent downstream consequences of *B. afzelii* acquisition during the larval blood meal, whereby early pathogen colonization induces long-lasting restructuring of the microbiota that persists into the nymphal stage. Under this scenario, differences in network cohesion would reflect pathogen-driven community reorganization rather than pre-existing microbiome-mediated resistance. Importantly, because the microbiome was characterized in nymphs several weeks after acquisition and the larval microbiome was not measured at the time of or immediately following pathogen acquisition, the present data do not allow discrimination between these two hypotheses.

Notably, across all networks, significant co-occurrence correlations were dominated by positive correlations. This may reflect the dominance of cooperative or neutral interactions in the tick microbiome. Such interaction structures imply that microbiome effects on pathogen colonization may operate predominantly through indirect mechanisms, including metabolic constraints or immune modulation (Mateos-Hernandez et al., 2025), rather than through direct antagonistic interactions, as also reported in mosquito and human systems (Li et al., 2018; Schmidt and Engel, 2021).

Our results highlight a dynamic assembly process where larval microbiota displays high cohesiveness, feeding leads to initial disruption (control), and subsequent exposure to *Borrelia* induces either complex restructuring (refractory) or more clustered reorganization (permissive). These divergent topologies suggest that infection susceptibility may be linked to the structure and redundancy of microbial networks, with more complex and modular communities potentially conferring resistance to colonization. Maitre et al. (2023) further support this hypothesis by demonstrating that pathogens like *Rickettsia* influence microbial network assembly in ticks, shaping microbiota interactions rather than simply replacing existing taxa. Their study found that, despite having low centrality, *Rickettsia* played a major role in structuring the microbial network, affecting bacterial interactions and stability. The removal of *Rickettsia* significantly altered microbiota structure, indicating that certain bacteria act as keystone taxa for microbial stability. Importantly, these associations do not allow discrimination between cause and consequence, and both microbiome-mediated resistance and pathogen-driven network restructuring remain compatible with the observed patterns.

Furthermore, our analysis confirmed that the method of dysbiosis, rinsing tick eggs with either bleach or water, disrupts microbial community assembly. However, this perturbation does not irreversibly compromise microbiota maturation after the blood meal and the subsequent larva-to-nymph moult. The resulting nymphs, particularly those refractories to *Borrelia*, exhibited microbial networks with re-established connectivity and modularity, closely resembling control nymphs. These findings underscore the capacity of the tick microbiota to reorganize and recover structural stability following transient compositional disturbances. These findings suggest that disrupting the initial microbiota can trigger a reorganization of microbial associations, potentially promoting network plasticity or even resilience (Fernández-Ruiz et al., 2023; Shade et al., 2012). However, in the presence of a pathogen, this reorganization can also lead to reduced modularity and fragmentation, as seen in the permissive-dysbiosed nymphs. This suggests that Borrelia colonization is not a passive process but instead actively alters the microbiota (Wu-Chuang et al., 2023), likely facilitating its own persistence by reducing microbial competition.

Boulanger et al. (2023) demonstrated that tick feeding disrupts the microbiomes of both the ticks and hosts, leading to microbiota shifts that may facilitate pathogen transmission. If tick feeding itself alters microbiota composition, it could be likely that Borrelia takes advantage of this disruption to establish itself within the tick gut. Our study builds upon these findings by showing that even in the absence of Borrelia colonization, microbial community assembly is altered, reinforcing the idea that exposure to an infected host alone drives microbial shifts. However, refractory nymphs appear to retain a more resilient microbial network, which may be characteristic of outcomes in which *Borrelia* establishment is not detected.

*Staphylococcus* emerged as a taxon of particular interest due to its differential role in microbiota structure and potential influence on *Borrelia* colonization. We detected this genus in larvae that hatched from both bleach-treated and water-treated eggs, with comparable prevalence across groups (12.6 % in larvae that hatched from water-rinsed eggs versus 15.5 % in larvae that hatched from bleached eggs) and higher relative abundance in nymphal stages. The presence of *Staphylococcus* in unfed larvae, regardless of decontamination treatment, alongside previous evidence that bleach and ethanol reduce surface contaminants while preserving internal microbial communities, supports the interpretation of *Staphylococcus* as a resident component of the tick microbiota rather than an external contaminant (Binetruy et al., 2019; Hoffmann et al., 2020; Du et al., 2023).

In permissive nymphs, we observed a positive correlation between the relative abundances of *Staphylococcus* and *Borrelia*, suggesting co-occurrence rather than mutual exclusion. Notably, *in silico* removal of *Staphylococcus* significantly reduced network robustness in permissive nymphs, indicating that this taxon becomes structurally important for maintaining connectivity in these communities. This finding suggests that *Staphylococcus* is integrated into an infection-associated module that accumulates topological centrality, leading to a network assembly that is increasingly dependent on specific taxa and therefore less resilient to targeted perturbations. This role is unlikely to stem from direct antagonism. Instead, two non-mutually exclusive hypotheses may explain this association. First, *Staphylococcus* possesses catalase and other antioxidant enzymes capable of neutralizing reactive oxygen species (ROS), which could indirectly protect *Borrelia* within an inflamed gut microenvironment (Gaupp et al., 2012; Da Cruz Nizer et al., 2024). Second, the presence of *Borrelia* can remodel the tick gut niche through modulation of host gene expression and tissue environment (e.g., through tick-encoded factors like PIXR and changes in gut gene expression) (Narasimhan et al., 2017) potentially altering the ecological role of *Staphylococcus* from a redundant connector to a structurally influential taxon within permissive networks.

Our analyses indicate that *Staphylococcus* acts as a context-dependent

taxon whose influence on network structure is determined by the underlying community assembly. In larvae with a natural microbiota (water-treated), *Staphylococcus* was consistently present, yet its removal did not produce measurable changes in network robustness, indicating that larval networks retain sufficient topological redundancy to maintain stability independently of this taxon. In permissive-normal nymphal networks, *Staphylococcus* became structurally important, as its removal led to significant reductions in network robustness, revealing a strong dependency on this central taxon and a loss of redundancy within the community. Under dysbiosis, its role diverged across assemblies: in control-dysbiosed nymphs, removal of *Staphylococcus* resulted in increased robustness, suggesting that its presence constrained network resilience, whereas in refractory-dysbiosed nymphs, its removal did not significantly affect robustness, consistent with a highly redundant and stable assembly. Together, these findings support the notion that colonization resistance is not driven by the abundance or centrality of *Staphylococcus* per se, but rather emerges from robust, redundantly connected network architectures. Consequently, targeted interventions involving this taxon should be interpreted within the specific network context in which it operates. Experimental interventions offer further insight into this context-dependent role. Anti-*Staphylococcus* vaccination significantly altered microbiota composition in *I. ricinus* ticks (Maitre et al., 2025), yet did not affect *Borrelia* acquisition, reinforcing the idea that *Staphylococcus* may modulate network structure rather than exert direct antimicrobial effects. In contrast, vaccination against *Escherichia* reduced *Borrelia* colonization (Wu-Chuang et al., 2023), highlighting how targeting specific microbial taxa can modulate infection outcomes through shifts in network topology and function. These findings align with previous findings in *A. phagocytophilum*-infected *I. scapularis* ticks, where the pathogen presence was associated with increased microbial modularity and reduced resilience (Abuin-Denis et al., 2024b) and reinforce the idea that pathogen acquisition is not solely a function of microbiota diversity, but rather the result of microbial network integrity and functional resilience.

If colonization resistance is primarily network-driven, interventions focused on maintaining microbial stability, rather than altering individual bacterial species, may be more effective in preventing Borrelia establishment in ticks. Additionally, understanding pathogen-induced microbiota shifts can provide insights into how Borrelia manipulates its vector environment. If Borrelia actively destabilizes tick microbial networks to enhance its own survival, future research could aim on blocking these interactions to reduce pathogen transmission.

We acknowledge that the tick microbiome is not the only determinant of pathogen acquisition. Pathogen strain variation, host immune status, and the spatial distribution of spirochetes in host skin all influence transmission success. It is plausible that some refractory nymphs failed to acquire *B. afzelii* due to host immune factors limiting transmission. Our goal was not to exclude these factors, but to explore whether microbiome structure covaries with colonization outcomes under realistic infection scenarios. Our findings suggest that microbial network architecture and functional pathways may offer additional explanatory power. Nevertheless, future studies using gnotobiotic models or controlled microbiota transplantation will be needed to disentangle causality.

## 5. Conclusion

This study demonstrates that microbiota network stability, rather than diversity alone, plays a key role in *B. afzelii* colonization resistance in *I. ricinus* ticks. While microbiome diversity did not differ significantly between ticks that acquired *Borrelia* and those that did not, network analysis revealed that ticks refractory to infection maintained stronger microbial connectivity and resilience, whereas permissive ticks exhibited weakened interactions and reduced network robustness. The presence of *Staphylococcus* as a central microbial node in refractory ticks suggests it may contribute to microbiota stability rather than direct competition with *Borrelia*. These findings suggest that colonization resistance to *B. afzelii* is not solely driven by specific taxa, but by the capacity of the microbiota to preserve topological integrity under ecological stress. Understanding how *Borrelia* acquisition is associated with changes in microbiota community assembly could lead to new strategies for reducing vector competence by reinforcing microbial network stability, shifting the focus from pathogen removal to strengthening microbiome resilience as a potential disease control approach.

## Funding sources

BIPAR was funded by the French Government's Investissement d'Avenir program, Laboratoire d'Excellence "Integrative Biology of Emerging Infectious Diseases" (grant no ANR-10-LABX-62-IBEID).

## Ethics statement

No experiments involving animals or humans were conducted in this study. The data used were obtained from publicly available sources, and no ethical approval was required.

## Declaration of generative AI and AI-assisted technologies in the manuscript preparation process

Artificial intelligence (AI) tools (i.e., ChatGPT) were used to assist with language editing and improving the flow of the manuscript. AI was not used to generate original ideas, analyze data, or draw scientific conclusions. The authors take full responsibility for the content, accuracy, and integrity of the manuscript.

**Supplementary Table S1:** List of taxa detected across normal larvae and dysbiosed larvae.

**Supplementary Table S2:** p-values of the network robustness comparisons between dysbiosed and normal larval network using *t*-test.

## CRediT authorship contribution statement

**Lianet Abuin-Denis:** Writing – review & editing, Writing – original draft, Visualization, Methodology, Formal analysis, Conceptualization. **Lourdes Mateos-Hernández:** Writing – review & editing, Data curation. **Apolline Maitre:** Writing – review & editing. **Alejandra Wu-Chuang:** Writing – review & editing. **Myriam Kratou:** Writing – review & editing. **Salma Kaoutar Abdelali:** Writing – review & editing. **Ana Laura Cano-Argüelles:** Writing – review & editing. **Štefánia Skičková:** Writing – review & editing, Visualization, Methodology, Formal analysis. **Dasiel Obregon:** Writing – review & editing, Software. **Alina Rodríguez-Mallon:** Writing – review & editing, Supervision. **Alejandro Cabezas-Cruz:** Writing – review & editing, Writing – original draft, Conceptualization.

## Declaration of competing interest

Given their role as Guest Editor, Alina Rodríguez-Mallon had no involvement in the peer review of this article and had no access to information regarding its peer review. Full responsibility for the editorial process for this article was delegated to another journal editor.

## Supplementary materials

Supplementary material associated with this article can be found, in the online version, at doi:10.1016/j.ttbdis.2026.102613.

## Data availability

The data used in this study are available in the NCBI Sequence Read Archive (SRA) under BioProject accession number PRJNA732915.

## References


Abuin-Denis, L., Piloto-Sardiñas, E., Maitre, A., Wu-Chuang, A., Mateos-Hernández, L., Gonzaga Paulino, P., Bello, Y., Ledesma Bravo, F., Alvarez Gutierrez, A., Rodríguez Fernández, R., Fuentes Castillo, A., Méndez Mellor, L., Foucault-Simonin, A., Obregon, D., Estrada-García, M.P., Rodriguez-Mallon, A., Cabezas-Cruz, A., 2024a. Differential nested patterns of *Anaplasma marginale* and *coxiella*-like endosymbiont across *Rhipicephalus microplus* ontogeny. Microbiol. Res. 286, 127790. https://doi.org/10.1016/j.micres.2024.127790.

Abuin-Denis, L., Piloto-Sardiñas, E., Maitre, A., Wu-Chuang, A., Mateos-Hernández, L., Obregón, D., Corona-González, B., Fogaça, A.C., Palinauskas, V., Aželytė, J., Rodriguez-Mallon, A., Cabezas-Cruz, A., 2024b. Exploring the impact of *Anaplasma phagocytophilum* on colonization resistance of *Ixodes scapularis* microbiota using network node manipulation. Curr. Res. Parasitol. Vector-Borne Dis. 5, 100177. https://doi.org/10.1016/j.crpvbd.2024.100177.

Aitchison, J., 1982. The statistical analysis of compositional data. J. R. Stat. Soc. Ser. B Stat. Methodol. 44, 139–160. https://doi.org/10.1111/j.2517-6161.1982.tb01195.x.

Aželytė, J., Maitre, A., Abuin-Denis, L., Piloto-Sardiñas, E., Wu-Chuang, A., Žiegytė, R., Mateos-Hernández, L., Obregón, D., Cabezas-Cruz, A., Palinauskas, V., 2024. Impact of *plasmodium relictum* infection on the colonization resistance of bird gut microbiota: a preliminary study. Pathogens 13, 91. https://doi.org/10.3390/pathogens13010091.

Bastian, M., Heymann, S., Jacomy, M., 2009. Gephi: An open Source Software For Exploring and Manipulating Networks. WebAtlas.

Binetruy, F., Dupraz, M., Buysse, M., Duron, O., 2019. Surface sterilization methods impact measures of internal microbial diversity in ticks. Parasit. Vectors. 12, 268. https://doi.org/10.1186/s13071-019-3517-5.

Bolyen, E., Rideout, J.R., Dillon, M.R., Bokulich, N.A., Abnet, C.C., Al-Ghalith, G.A., Alexander, H., Alm, E.J., Arumugam, M., Asnicar, F., Bai, Y., Bisanz, J.E., Bittinger, K., Brejnrod, A., Brislawn, C.J., Brown, C.T., Callahan, B.J., Caraballo-Rodríguez, A.M., Chase, J., Cope, E.K., Da Silva, R., Diener, C., Dorrestein, P.C., Douglas, G.M., Durall, D.M., Duvallet, C., Edwardson, C.F., Ernst, M., Estaki, M., Fouquier, J., Gauglitz, J.M., Gibbons, S.M., Gibson, D.L., Gonzalez, A., Gorlick, K., Guo, J., Hillmann, B., Holmes, S., Holste, H., Huttenhower, C., Huttley, G.A., Janssen, S., Jarmusch, A.K., Jiang, L., Kaehler, B.D., Kang, K.B., Keefe, C.R., Keim, P., Kelley, S.T., Knights, D., Koester, I., Kosciolek, T., Kreps, J., Langille, M.G.I., Lee, J., Ley, R., Liu, Y.-X., Loftfield, E., Lozupone, C., Maher, M., Marotz, C., Martin, B.D., McDonald, D., McIver, L.J., Melnik, A.V., Metcalf, J.L., Morgan, S.C., Morton, J.T., Naimey, A.T., Navas-Molina, J.A., Nothias, L.F., Orchanian, S.B., Pearson, T., Peoples, S.L., Petras, D., Preuss, M.L., Pruesse, E., Rasmussen, L.B., Rivers, A., Robeson, M.S., Rosenthal, P., Segata, N., Shaffer, M., Shiffer, A., Sinha, R., Song, S.J., Spear, J.R., Swafford, A.D., Thompson, L.R., Torres, P.J., Trinh, P., Tripathi, A., Turnbaugh, P.J., Ul-Hasan, S., van der Hooft, J.J.J., Vargas, F., Vázquez-Baeza, Y., Vogtmann, E., von Hippel, M., Walters, W., Wan, Y., Wang, M., Warren, J., Weber, K. C., Williamson, C.H.D., Willis, A.D., Xu, Z.Z., Zaneveld, J.R., Zhang, Y., Zhu, Q., Knight, R., Caporaso, J.G., 2019. Reproducible, interactive, scalable and extensible microbiome data science using QIIME 2. Nat. Biotechnol. 37, 852–857. https://doi.org/10.1038/s41587-019-0209-9.

Boulanger, N., Insonere, J.-L.-M., Van Blerk, S., Barthel, C., Serres, C., Rais, O., Roulet, A., Servant, F., Duron, O., Lelouvier, B., 2023. Cross-alteration of murine skin and tick microbiome concomitant with pathogen transmission after *Ixodes ricinus* bite. Microbiome 11, 250. https://doi.org/10.1186/s40168-023-01696-7.

Bray, J.R., Curtis, J.T., 1957. An ordination of the upland forest communities of Southern Wisconsin. Ecol. Monogr. 27, 325–349. https://doi.org/10.2307/1942268.

Callahan, B.J., McMurdie, P.J., Holmes, S.P., 2017. Exact sequence variants should replace operational taxonomic units in marker-gene data analysis. ISME J 11, 2639–2643. https://doi.org/10.1038/ismej.2017.119.

Callahan, B.J., McMurdie, P.J., Rosen, M.J., Han, A.W., Johnson, A.J.A., Holmes, S.P., 2016. DADA2: high-resolution sample inference from Illumina amplicon data. Nat. Methods. 13, 581–583. https://doi.org/10.1038/nmeth.3869.

Da Cruz Nizer, W.S., Adams, M.E., Allison, K.N., Montgomery, M.C., Mosher, H., Cassol, E., Overhage, J., 2024. Oxidative stress responses in biofilms. Biofilm 7, 100203. https://doi.org/10.1016/j.bioflm.2024.100203.

de la Fuente, J., Antunes, S., Bonnet, S., Cabezas-Cruz, A., Domingos, A.G., Estrada-Peña, A., Johnson, N., Kocan, K.M., Mansfield, K.L., Nijhof, A.M., Papa, A., Rudenko, N., Villar, M., Alberdi, P., Torina, A., Ayllón, N., Vancova, M., Golovchenko, M., Grubhoffer, L., Caracappa, S., Fooks, A.R., Gortazar, C., Rego, R.O. M., 2017. Tick-pathogen interactions and vector competence: identification of molecular drivers for Tick-borne diseases. Front. Cell. Infect. Microbiol. 7, 14–26. https://doi.org/10.3389/fcimb.2017.00114.

Du, L.-F., Zhang, M.-Z., Yuan, T.-T., Ni, X.-B., Wei, W., Cui, X.-M., Wang, N., Xiong, T., Zhang, J., Pan, Y.-S., Zhu, D.-Y., Li, L.-J., Xia, L.-Y., Wang, T.-H., Wei, R., Liu, H.-B., Sun, Y., Zhao, L., Lam, T.T.-Y., Cao, W.-C., Jia, N., 2023. New insights into the impact of microbiome on horizontal and vertical transmission of a tick-borne pathogen. Microbiome 11, 50. https://doi.org/10.1186/s40168-023-01485-2.

Faith, D.P., 1992. Conservation evaluation and phylogenetic diversity. Biol. Conserv. 61, 1–10. https://doi.org/10.1016/0006-3207(92)91201-3.

Fernandes, A.D., Macklaim, J.M., Linn, T.G., Reid, G., Gloor, G.B., 2013. ANOVA-like differential expression (ALDEx) analysis for mixed population RNA-seq. PLoS ONE 8, e67019. https://doi.org/10.1371/journal.pone.0067019.

Fernández-Ruiz, N., Pinecki-Socias, S., Estrada-Peña, A., Wu-Chuang, A., Maitre, A., Obregón, D., Cabezas-Cruz, A., De Blas, I., Nijhof, A.M., 2023. Decontamination protocols affect the internal microbiota of ticks. Parasit. Vectors. 16, 189. https://doi.org/10.1186/s13071-023-05812-2.

Friedman, J., Alm, E.J., 2012. Inferring correlation networks from genomic survey data. PLoS Comput. Biol. 8, e1002687. https://doi.org/10.1371/journal.pcbi.1002687.

Gaupp, R., Ledala, N., Somerville, G.A., 2012. Staphylococcal response to oxidative stress. Front. Cell. Infect. Microbiol. 2, 37–55. https://doi.org/10.3389/fcimb.2012.00033.

Genné, D., Rossel, M., Sarr, A., Battilotti, F., Rais, O., Rego, R.O.M., Voordouw, M.J., 2021. Competition between strains of *Borrelia afzelii* in the host tissues and consequences for transmission to ticks. ISME J 15, 2390–2400. https://doi.org/10.1038/s41396-021-00939-5.

Genné, D., Sarr, A., Gomez-Chamorro, A., Durand, J., Cayol, C., Rais, O., Voordouw, M. J., 2018. Competition between strains of *Borrelia afzelii* inside the rodent host and the tick vector. Proc. R. Soc. B Biol. Sci. 285, 20181804. https://doi.org/10.1098/rspb.2018.1804.

Genné, D., Sarr, A., Rais, O., Voordouw, M.J., 2019. Competition between strains of *Borrelia afzelii* in immature *Ixodes ricinus* ticks is not affected by season. Front. Cell. Infect. Microbiol. 9, 431. https://doi.org/10.3389/fcimb.2019.00431.

Hamilton, P.T., Maluenda, E., Sarr, A., Belli, A., Hurry, G., Duron, O., Plantard, O., Voordouw, M.J., 2021. *Borrelia afzelii* infection in the rodent host has dramatic effects on the bacterial microbiome of *Ixodes ricinus* ticks. Appl. Environ. Microbiol. 87. https://doi.org/10.1128/AEM.00641-21 e00641-21.

Heylen, D.J.A., Müller, W., Vermeulen, A., Sprong, H., Matthysen, E., 2015. Virulence of recurrent infestations with *Borrelia*-infected ticks in a *Borrelia*-amplifying bird. Sci. Rep. 5, 16150. https://doi.org/10.1038/srep16150.

Hoffmann, A., Fingerle, V., Noll, M., 2020. Analysis of tick surface decontamination methods. Microorganisms 8, 987. https://doi.org/10.3390/microorganisms8070987.

Jacquet, M., Margos, G., Fingerle, V., Voordouw, M.J., 2016. Comparison of the lifetime host-to-tick transmission between two strains of the Lyme disease pathogen *Borrelia afzelii*. Parasit. Vectors. 9, 645. https://doi.org/10.1186/s13071-016-1929-z.

Katoh, K., 2002. MAFFT: a novel method for rapid multiple sequence alignment based on fast fourier transform. Nucleic Acids Res 30, 3059–3066. https://doi.org/10.1093/nar/gkf436.

Knight, R., Vrbanac, A., Taylor, B.C., Aksenov, A., Callewaert, C., Debelius, J., Gonzalez, A., Kosciolek, T., McCall, L.-I., McDonald, D., Melnik, A.V., Morton, J.T., Navas, J., Quinn, R.A., Sanders, J.G., Swafford, A.D., Thompson, L.R., Tripathi, A., Xu, Z.Z., Zaneveld, J.R., Zhu, Q., Caporaso, J.G., Dorrestein, P.C., 2018. Best practices for analysing microbiomes. Nat. Rev. Microbiol. 16, 410–422. https://doi.org/10.1038/s41579-018-0029-9.

Kurtz, Z.D., Müller, C.L., Miraldi, E.R., Littman, D.R., Blaser, M.J., Bonneau, R.A., 2015. Sparse and compositionally robust inference of microbial ecological networks. PLOS Comput. Biol. 11, e1004226. https://doi.org/10.1371/journal.pcbi.1004226.

Kwan, J.Y., Griggs, R., Chicana, B., Miller, C., Swei, A., 2017. Vertical vs. horizontal transmission of the microbiome in a key disease vector, Ixodes pacificus. Mol. Ecol. 26, 6578–6589. https://doi.org/10.1111/mec.14391.

Lhomme, S., 2015. Analyse spatiale de la structure des réseaux techniques dans un contexte de risques. Cybergeo. https://doi.org/10.4000/cybergeo.26763.

Li, Q., Zhang, B., Yang, X., Ge, Q., 2018. Deterioration-associated microbiome of stone monuments: structure, variation, and assembly. Appl. Environ. Microbiol. 84. https://doi.org/10.1128/AEM.02680-17 e02680-17.

Maitre, A., Mateos-Hernandez, L., Kratou, M., Egri, N., Maye, J., Juan, M., Hodžić, A., Obregón, D., Abuin-Denis, L., Piloto-Sardinas, E., Fogaça, A.C., Cabezas-Cruz, A., 2025. Effects of live and peptide-based antimicrobiota vaccines on *Ixodes ricinus* fitness, microbiota, and acquisition of tick-borne pathogens. Pathogens 14, 206. https://doi.org/10.3390/pathogens14030206.

Maitre, A., Wu-Chuang, A., Mateos-Hernández, L., Piloto-Sardiñas, E., Foucault-Simonin, A., Cicculli, V., Moutailler, S., Paoli, J., Falchi, A., Obregón, D., Cabezas-Cruz, A., 2023. Rickettsial pathogens drive microbiota assembly in *hyalomma marginatum* and *rhipicephalus bursa* ticks. Mol. Ecol. mec., 17058 https://doi.org/10.1111/mec.17058.

Mateos-Hernandez, L., Abuin-Denis, L., Wu-Chuang, A., Maitre, A., Roháčková, H., Rego, R.O.M., Piloto-Sardiñas, E., Valdes, J., Porcelli, S., Heckmann, A., Moutailler, S., Lucas-Torres, C., Moos, M., Opekar, S., Kratou, M., Obregon, D., Cabezas-Cruz, A., 2025. Antimicrobiota vaccine induces lysine-mediated modulation of tick immunity affecting *Borrelia* colonization. FEMS Microbiol. Ecol. 101, fiaf082. https://doi.org/10.1093/femsec/fiaf082.

Mateos-Hernández, L., Obregón, D., Wu-Chuang, A., Maye, J., Bornères, J., Versillé, N., de la Fuente, J., Díaz-Sánchez, S., Bermúdez-Humarán, L.G., Torres-Maravilla, E., Estrada-Peña, A., Hodžić, A., Šimo, L., Cabezas-Cruz, A., 2021. Anti-microbiota vaccines modulate the tick microbiome in a taxon-specific manner. Front. Immunol. 12, 704621. https://doi.org/10.3389/fimmu.2021.704621.

Narasimhan, S., Rajeevan, N., Graham, M., Wu, M.-J., DePonte, K., Marion, S., Masson, O., O'Neal, A.J., Pedra, J.H.F., Sonenshine, D.E., Fikrig, E., 2022. Tick transmission of *Borrelia burgdorferi* to the murine host is not influenced by environmentally acquired midgut microbiota. Microbiome 10, 173. https://doi.org/10.1186/s40168-022-01378-w.

Narasimhan, S., Rajeevan, N., Liu, L., Zhao, Y.O., Heisig, J., Pan, J., Eppler-Epstein, R., Deponte, K., Fish, D., Fikrig, E., 2014. Gut microbiota of the tick vector *ixodes scapularis* modulate colonization of the Lyme disease spirochete. Cell Host Microbe 15, 58–71. https://doi.org/10.1016/j.chom.2013.12.001.

Narasimhan, S., Schuijt, T.J., Abraham, N.M., Rajeevan, N., Coumou, J., Graham, M., Robson, A., Wu, M.-J., Daffre, S., Hovius, J.W., Fikrig, E., 2017. Modulation of the tick gut milieu by a secreted tick protein favors *Borrelia burgdorferi* colonization. Nat. Commun. 8, 184. https://doi.org/10.1038/s41467-017-00208-0.

Nearing, J.T., Douglas, G.M., Hayes, M.G., MacDonald, J., Desai, D.K., Allward, N., Jones, C.M.A., Wright, R.J., Dhanani, A.S., Comeau, A.M., Langille, M.G.I., 2022.

Microbiome differential abundance methods produce different results across 38 datasets. Nat. Commun. 13, 342. https://doi.org/10.1038/s41467-022-28034-z.
Obregon, D., Maitre, A., Piloto-Sardiñas, E., Wu-Chuang, A., Abuin-Denis, L., Cano-Argüelles, A.L., Aželytė, J., Corona-Guerrero, I., Mateos-Hernández, L., Kratou, M., Skičková, Š., Svobodová, K., Cabezas-Cruz, A., 2025. Decoding microbial community assembly: insights on vectors of infectious diseases. Annu. Rev. Microbiol. 79, 547–572. https://doi.org/10.1146/annurev-micro-082024-094943.
Oksanen, J., Blanchet, F.G., Friendly, M., Kindt, R., Legendre, P., McGlinn, D., Minchin, P., O'Hara, R., Simpson, G., Solymos, P., Stevens, M., Szöcs, E., Wagner, H., 2020. vegan community ecology package version 2.5-7 November 2020.
Peschel, S., Müller, C.L., von Mutius, E., Boulesteix, A.-L., Depner, M., 2021. NetCoMi: network construction and comparison for microbiome data in R. Brief. Bioinform. 22, bbaa290. https://doi.org/10.1093/bib/bbaa290.
Pielou, E.C., 1966. The measurement of diversity in different types of biological collections. J. Theor. Biol. 13, 131–144. https://doi.org/10.1016/0022-5193(66)90013-0.
Piesman, J., Gern, L., 2004. Lyme borreliosis in Europe and North America. Parasitology 129, S191–S220. https://doi.org/10.1017/S0031182003004694.
Piloto-Sardiñas, E., Abuin-Denis, L., Maitre, A., Foucault-Simonin, A., Corona-González, B., Díaz-Corona, C., Roblejo-Arias, L., Mateos-Hernández, L., Marrero-Perera, R., Obregon, D., Svobodová, K., Wu-Chuang, A., Cabezas-Cruz, A., 2024. Dynamic nesting of *anaplasma marginale* in the microbial communities of *rhipicephalus microplus*. Ecol. Evol. 14, e11228. https://doi.org/10.1002/ece3.11228.
Price, M.N., Dehal, P.S., Arkin, A.P., 2010. FastTree 2 – approximately maximum-likelihood trees for large alignments. PLoS ONE 5, e9490. https://doi.org/10.1371/journal.pone.0009490.
Prodan, A., Tremaroli, V., Brolin, H., Zwinderman, A.H., Nieuwdorp, M., Levin, E., 2020. Comparing bioinformatic pipelines for microbial 16S rRNA amplicon sequencing. PLOS ONE 15, e0227434. https://doi.org/10.1371/journal.pone.0227434.
Quast, C., Pruesse, E., Yilmaz, P., Gerken, J., Schweer, T., Yarza, P., Peplies, J., Glöckner, F.O., 2013. The SILVA ribosomal RNA gene database project: improved data processing and web-based tools. Nucleic Acids Res 41, D590–D596. https://doi.org/10.1093/nar/gks1219.
R Core Team, 2023. R: A language and Environment For Statistical Computing. R Foundation for Statistical Computing.
Radolf, J.D., Caimano, M.J., Stevenson, B., Hu, L.T., 2012. Of ticks, mice and men: understanding the dual-host lifestyle of Lyme disease spirochaetes. Nat. Rev. Microbiol. 10, 87–99. https://doi.org/10.1038/nrmicro2714.
Real, R., Vargas, J.M., 1996. The probabilistic basis of Jaccard's Index of Similarity. Syst. Biol. 45, 380–385. https://doi.org/10.1093/sysbio/45.3.380.
Röttjers, L., Vandeputte, D., Raes, J., Faust, K., 2021. Null-model-based network comparison reveals core associations. ISME Commun 1, 36. https://doi.org/10.1038/s43705-021-00036-w.
RStudio Team, 2020. RStudio: integrated development for R. [WWW Document]. URL http://www.rstudio.org/.
Schmidt, K., Engel, P., 2021. Mechanisms underlying gut microbiota–host interactions in insects. J. Exp. Biol. 224, jeb207696. https://doi.org/10.1242/jeb.207696.
Shade, A., Peter, H., Allison, S.D., Baho, D.L., Berga, M., Bürgmann, H., Huber, D.H., Langenheder, S., Lennon, J.T., Martiny, J.B.H., Matulich, K.L., Schmidt, T.M., Handelsman, J., 2012. Fundamentals of microbial community resistance and resilience. Front. Microbiol. 3, 166–184. https://doi.org/10.3389/fmicb.2012.00417.
Skičková, Š., Svobodová, K., Maitre, A., Wu-Chuang, A., Abuin-Denis, L., Piloto-Sardiñas, E., Obregon, D., Majláth, I., Majláthová, V., Krejčí, A., Cabezas-Cruz, A., 2024. Differential impact of *paenibacillus* infection on the microbiota of *Varroa destructor* and *Apis mellifera*. Heliyon 10, e39384. https://doi.org/10.1016/j.heliyon.2024.e39384.
Wu-Chuang, A., Mateos-Hernandez, L., Maitre, A., Rego, R.O.M., Šíma, R., Porcelli, S., Rakotobe, S., Foucault-Simonin, A., Moutailler, S., Palinauskas, V., Aželytė, J., Símo, L., Obregon, D., Cabezas-Cruz, A., 2023. Microbiota perturbation by anti-microbiota vaccine reduces the colonization of *Borrelia afzelii* in *Ixodes ricinus*. Microbiome 11, 151. https://doi.org/10.1186/s40168-023-01599-7.
Yarza, P., Yilmaz, P., Pruesse, E., Glöckner, F.O., Ludwig, W., Schleifer, K.-H., Whitman, W.B., Euzéby, J., Amann, R., Rosselló-Móra, R., 2014. Uniting the classification of cultured and uncultured bacteria and archaea using 16S rRNA gene sequences. Nat. Rev. Microbiol. 12, 635–645. https://doi.org/10.1038/nrmicro3330.
Zolnik, C.P., Prill, R.J., Falco, R.C., Daniels, T.J., Kolokotronis, S., 2016. Microbiome changes through ontogeny of a tick pathogen vector. Mol. Ecol. 25, 4963–4977. https://doi.org/10.1111/mec.13832.